Paoli *et al. Genome Medicine* (2026) 18:27
https://doi.org/10.1186/s13073-026-01603-3

Genome Medicine

METHODOLOGY Open Access

A computational framework for sensitive tumor detection and accurate subtyping using shallow cell-free DNA methylome sequencing

Marta Paoli[1,2†], Francesca Galardi[3†], Agostina Nardone[3], Chiara Biagioni[2], Dario Romagnoli[2,4], Samantha Di Donato[2], Gian Marco Franceschini[1], Luca Livraghi[2], Marta Pestrin[5], Giuseppina Sanna[6], Emanuela Risi[2], Ilenia Migliaccio[3], Erica Moretti[2], Luca Malorni[2,3], Laura Biganzoli[2†], Francesca Demichelis[1†] and Matteo Benelli[2,4*†]

Abstract

Plasma circulating tumor DNA (ctDNA) enables non-invasive monitoring of metastatic cancer. However, the detection of low tumor content (TC) via tumor tissue-agnostic approaches remains challenging. We introduce METER, a computational strategy exploiting tumor-type specific DNA methylation patterns for sensitive ctDNA detection, accurate quantification, and subtyping from plasma low-pass (0.5-1x) whole-methylome sequencing. In longitudinal samples from metastatic breast cancer patients, METER demonstrated a stronger association with clinical outcomes than both state-of-the-art ctDNA methods and matched circulating tumor cell (CTC) counts, even at TC below 3%. METER (https://github.com/caos-lab-unifi/METER) integrates TC estimation and subtyping in a single framework, enabling sensitive and accurate analyses for precision oncology.

Keywords Liquid biopsy, DNA methylation, Circulating tumor DNA, Biomarker, Methylome, Breast cancer, Tumor subtyping, Estrogen receptor, Precision oncology

Background

Cell-free DNA (cfDNA)-based liquid biopsy is becoming critical for clinical management of cancer patients [1, 2] and, supported by a large body of clinical studies, is expected to play a major role in oncological practice in the near future. In the metastatic setting, it can complement imaging to improve response monitoring [3], offering several advantages over traditional tissue biopsies. It is not limited by challenging-to-access metastatic sites, and its minimal invasiveness enables serial sampling for real-time disease monitoring and timely treatment interventions [4]. A primary strategy for these applications involves evaluating the presence and proportion of circulating tumor DNA (ctDNA) within the total cell-free

†Marta Paoli and Francesca Galardi are co-first authorship.

†Laura Biganzoli, Francesca Demichelis and Matteo Benelli are co-senior authorship.

*Correspondence:
Matteo Benelli
matteo.benelli@unifi.it
[1]Department of Cellular, Computational and Integrative Biology, University of Trento, Trento, Italy
[2]Department of Medical Oncology, Hospital of Prato, Azienda USL Toscana Centro, Prato, Italy
[3]Translational Research Unit, Department of Medical Oncology, Hospital of Prato, Azienda USL Toscana Centro, Prato, Italy
[4]Department of Experimental and Clinical Biomedical Sciences, University of Florence, Florence, Italy
[5]Medical Oncology Unit, Azienda Sanitaria Universitaria Giuliano Isontina, Gorizia, Italy
[6]Medical Oncology, Ospedale Civile SS Annunziata, Sassari, Italy

DNA (cfDNA) from patients' blood samples, referred to as tumor content (TC). Indeed, TC has emerged as an independent prognostic biomarker in various cancers, including breast cancer (BC) [5, 6], and as a powerful tool for monitoring disease during treatment [7]. Elevated TC levels are associated with relevant molecular features such as actionable variants and high mutational and copy number burden [8, 9]. The detection of plasma ctDNA may indicate poor response to treatment and a higher risk of early disease progression [1]. Moreover, ctDNA profiling may facilitate the monitoring of tumor phenotypic transformations and the emergence of molecular resistance mechanisms, overcoming challenges associated with metastatic biopsies and intra-tumoral heterogeneity [10, 11]. Improving TC analysis through scalable and robust methods is, therefore, a priority in precision oncology, enabling advancements in real-time disease monitoring and treatment optimization. One of the most common and effective strategies for measuring TC consists in the analysis of copy number alterations (CNA) and somatic point mutations either from target sequencing [12–15] or low-pass whole genome sequencing (lpWGS) by ichorCNA [16]. lpWGS has several advantages compared to other approaches based on the analysis of CNA or circulating mutations from targeted assays [17, 18]. First, it requires a low input DNA amount, enhancing the likelihood of successful analysis of liquid biopsy samples. Second, it is tumor-type agnostic, requiring no prior information about the molecular characteristics of the metastases shedding DNA in the circulation. Third, it is highly reproducible and cost-effective as it relies on well-established library preparation protocols, requires a few million reads, and utilizes state-of-the-art computational tools. However, its typical lower limit of TC detection of ~ 3% hinders its clinical applicability in challenging low-TC settings, such as metastatic disease monitoring at early treatment lines, where ctDNA detection is critical [19], failing to provide effective stratification of patients and hindering accurate identification of responders or early progressors. Further, low-pass CNA-based approaches are not ideal for assessing tumor-specific transcriptional programs that cannot be easily inferred by genomic alterations. Recent methods based on the analysis of genome-wide [10, 18, 20] or targeted DNA-methylation patterns [11, 18], epigenomics profiling [11, 21, 22], nucleosome positioning [23] and fragmentomics [17, 24] enable the analysis of both TC and relevant molecular features typically measurable in tumor tissues, such as histological and molecular subtypes. However, most of these epigenetics-based approaches, based on machine learning classifiers, require non-trivial experimental procedures, deep sequencing and prior knowledge of epigenetics features for their application.

We reasoned that the pervasiveness of cancer-related DNA-methylation patterns provides a robust signal, enabling ctDNA analysis through shallow, genome-wide sequencing approaches [25, 26]. Based on this, we developed METER (DNA-*MET*hylome Analys*ER*), a computational tool for ctDNA analysis from low-pass whole methylome sequencing of cfDNA samples. To evaluate METER's performance and its clinical relevance in the metastatic setting, we applied our method to 338 plasma samples from 124 patients with metastatic breast cancer (mBC) on early-line treatment, representing a challenging scenario spanning low TC levels from two independent cohorts. METER provided precise TC quantification and demonstrated enhanced sensitivity in TC detection, enabling effective disease monitoring and prognostic stratification. Additionally, it accurately inferred tumor subtypes, facilitating comprehensive analysis of tumor signals in circulation.

Methods

Study cohorts

The MIMESIS-1 and MIMESIS-2 studies enrolled patients with mBC coordinated at the Hospital of Prato (Italy) (CEAVC Em.2021-CEAVC study 15108, Area Vasta Toscana Centro and local Ethics Committee of the Hospital of Prato). The MIMESIS-1 dataset consists of 154 plasma samples from 30 healthy donors (Precision Medicine Group, LLC) and 59 patients with mBC [27, 28]. Most patients had hormone receptor positive/HER2 negative (HR+/HER2-) mBC (N = 36, 61%), while the remainder had HER2+ (N = 10, 17%) or triple negative breast cancer (TNBC) (N = 11, 19%). At study entry, 88% of patients (N = 52) had received fewer than 3 metastatic treatment lines (range 0–6), and 90% of patients (N = 53) had fewer than 4 metastatic sites at study entry (maximum 6). Main clinical characteristics are reported in Additional File 1: Table S1. Plasma samples were collected before initiating systemic therapy (pre-treatment baseline, BL; N = 59), after the first treatment cycle (day 1 of cycle 2, C2D1; N = 43), and at progression (Prog; N = 22). lpWGBS of plasma cell-free DNA was performed, yielding a median per-sample coverage of 0.8x (range 0.3–2.0x), corresponding to a median of 21 (range 7–50) million reads per sample. Circulating tumor cells (CTC) counts were previously determined for all patients, for 121 of 124 samples [29–31].

The MIMESIS-2 dataset includes 214 plasma samples from 65 patients with mBC. Most patients had HR+/HER2- mBC (N = 53, 82%), with HER2+ (6, 9%), TNBC (5, 8%), and one patient HR+ with unknown HER2 status. All patients had received no or one metastatic treatment line at study entry (48% and 52%, respectively), and 92% (N = 60) had fewer than four metastatic sites (range 1–6). Main clinical characteristics are reported

in Additional File 1: Table S2. Plasma samples were collected at 6 serial time points: BL ($N=62$), C2D1 ($N=62$), at the first three radiological evaluations (imaging, I1 ($N=3$), I2 ($N=26$), I3 ($N=23$)), and at Prog ($N=38$). lpWGBS of plasma cell-free DNA was performed, yielding a median per-sample coverage of 0.5x (range: 0.1–2x), corresponding to a median of ~14 million reads per sample (range: 4–48 million reads). The median follow-up was 31 months.

To evaluate METER in early-stage disease, we analyzed pre-operative plasma samples from four patients enrolled in the LIBIMET study (CEAVC Em.2024-CEAVC study 11252, Area Vasta Toscana Centro). LIBIMET is a multicenter, prospective study aimed at redefining prognostic stratification in colorectal cancer (CRC) using liquid biopsy–based biomarkers in patients with stage III and high-risk stage II disease [32].

Plasma samples collection, cfDNA extraction and library preparation

cfDNA was extracted by QIAmp Circulating Nucleic acid Kit (Qiagen) and quantified by Qubit (Qubit dsDNA High Sensitivity Kit, Life Technologies). cfDNA samples were stored at −80 °C until the bisulfite conversion. Approximately 20 ng (mean: 19.8 ng; range: 10.52 ng – 22.9 ng) of cfDNA was bisulfite converted using the EZ DNA Methylation-Lightning Kit (Zymo Research) according to the manufacturer's instructions. Samples with volume exceeded the 20µl input for conversion was concentrated by SpeedVac DNA130 (Thermo Fisher Scientific) at 35 °C. Bisulfite-converted cfDNA was eluted into 15µl of Low EDTA TE and used for library preparation. For MIMESIS-1 and LIBIMET, libraries were prepared using Accel-NGS Methyl-Seq DNA Library Kit (Swift Biosciences), Swift Normalase Unique Dual Indexing Primer Plates (Swift Biosciences) and KAPA HiFi HotStart Uracil (Roche), according to the manufacturer's instructions. For MIMESIS-2, libraries were prepared using the xGen™ Methyl-Seq Lib Prep (IDT), xGen Normalase UDI Primers plates (IDT) and KAPA HiFi HotStart Uracil (Roche) according to the manufacturer's instructions. 13 cycles of indexing PCR were conducted in order to achieve at least 300 ng of library product. Libraries' size distribution and concentration were analyzed respectively by Bioanalyzer DNA High Sensitivity Kit (Agilent) and Qubit (Qubit dsDNA High Sensitivity Kit, Life Technologies) before pooling and sequencing. Sequencing was performed with 15–25% PhiX (Illumina) spike-in at 2 × 150 bp on Illumina NovaSeq 6000.

In vitro and in silico artificial samples

In vitro artificial dilutions were generated mixing DNA extracted from luminal T47D BC cell line culture medium, as a surrogate of circulating tumor DNA (s-ctDNA), and a human mixed genomic DNA (PROMEGA) (0, 0.1, 0.5, 1, 2.5 and 5%). s-ctDNA was extracted by QIAmp Circulating Nucleic Acid Kit (Qiagen) and quantified by Qubit dsDNA High Sensitivity Kit, (Life Technologies). lpWGBS of these samples was generated as described in the previous section.

In silico artificial dilutions were generated by combining sequenced reads from WGBS of the luminal MCF7 breast cancer cell line, downloaded from Sequence Read Archive (SRA, GEO accession: GSM3336908) [33], with sequenced reads from pooled lpWGBS of 20 controls from the MIMESIS-1 dataset. Reads from these two sources were randomly sampled and mixed in proportions to simulate increasing TC and sequence coverage, using SAMtools version 1.16.1 [34]. Specifically, TC values ranging from 0 to 0.02 were simulated, generating 10 dilutions for each TC point, within distinct simulated coverage levels: 0.7x, 1.3x, 2.7x, and 4.0x. lpWGBS data from 20 out of 30 controls available were used to generate the dilutions, while data from the remaining 10 controls were pooled and subsequently used to generate 10 additional artificial controls, for each simulated coverage interval, through the random sampling of reads using SAMtools.

Processing of cfDNA-methylation data

Sequenced reads were processed through the 'methylseq' pipeline version 1.6.1 within the nf-core project [35] version 2.2, using the Bismark [36] workflow. Briefly, reads were aligned to the hg38 genome version using Bismark, trimmed using Accel-Ngs Methyl-seq specific parameters by Trim Galore [37]. Deduplication and methylation calls were obtained using Bismark. For in silico artificial dilutions, only the final step of methylation calls using Bismark was applied, as the sequenced reads used in creating the dilutions had already undergone processing.

Selection of informative BC-specific DMS and DMR

Rocker-meth [38] was applied with default parameters to identify BC-specific differentially methylated CpG sites (DMS) and regions (DMR) by comparing CpG β-values from WGBS of 30 BC tissue samples from the BASIS dataset [39] and 23 healthy cfDNA samples from Loyfer et al. [40].

The β-value of a CpG s in sample j is the fraction of methylated calls among all calls covering s, reflecting the proportion of cells in which the CpG is methylated [36, 41]:

$$\beta^{(\mathrm{j})}(\mathrm{s}) = \frac{{\mathrm{n_m}}^{(\mathrm{j})}(\mathrm{s})}{{\mathrm{n_m}}^{(\mathrm{j})}(\mathrm{s}) + {\mathrm{n_u}}^{(\mathrm{j})}(\mathrm{s})}$$

where $\mathrm{n_m^{(j)}}$ and ${n_u}^{(j)}$ are the methylated and unmethylated read counts, respectively.

Let $s = 1, \ldots, S$ index the CpG sites. We select those satisfying the following criteria:

$$\mathrm{AUC}(s) > 0.8\,(\mathrm{hyper})\; OR\; \mathrm{AUC}(s) < 0.2\,(\mathrm{hypo})$$

$$|\overline{\beta}_{\mathrm{tumor}}(s) - \overline{\beta}_{\mathrm{control}}(s)| \geq 0.4$$

$$\begin{array}{l}\left(Q3\left(\beta_{\mathrm{control}}(s)\right) < 0.1 \text{ AND } \left(\overline{\beta}_{\mathrm{tumor}}(s) - \overline{\beta}_{\mathrm{control}}(s)\right) > 0\right)(\mathrm{hyper}) \quad \text{OR} \\ \left(Q1\left(\beta_{\mathrm{control}}(s)\right) > 0.9 \text{ AND } \left(\overline{\beta}_{\mathrm{tumor}}(s) - \overline{\beta}_{\mathrm{control}}(s)\right) < 0\right)(\mathrm{hypo})\end{array}$$

where: $\mathrm{AUC}(s)$ is the area under the curve of a receiver operating characteristic (ROC) curve of a sites s separating tumor from control samples computed by Rocker-meth; $\overline{\beta}(s)$ is the mean β-value by group for site s; Q3 and Q1 are the third and first quartiles, respectively.

This procedure yielded a set D_{BC}, including ~45k hypermethylated and ~165k hypomethylated BC-specific DMS (Additional File 1: Table S3).

Let $g = 1, \ldots, G$ index the genomic regions. We select those satisfying the following criteria:

$$\mathrm{FDR}(g) < 0.05$$

$$|\overline{\beta}_{\mathrm{tumor}}(g) - \overline{\beta}_{\mathrm{control}}(g)| \geq 0.2$$

$$\begin{array}{l}\left(Q3\left(\beta_{\mathrm{control}}(g)\right) < 0.1 \text{ AND } \left(\overline{\beta}_{\mathrm{tumor}}(g) - \overline{\beta}_{\mathrm{control}}(g)\right) > 0\right)(\mathrm{hyper}) \quad \text{OR} \\ \left(Q1\left(\beta_{\mathrm{control}}(g)\right) > 0.9 \text{ AND } \left(\overline{\beta}_{\mathrm{tumor}}(g) - \overline{\beta}_{\mathrm{control}}(g)\right) < 0\right)(\mathrm{hypo})\end{array}$$

where: $\mathrm{FDR}(g)$ is the adjusted (Benjamini-Hochberg) p-value of a DMR g by Rocker-meth; $\overline{\beta}(g)$is computed as the mean of the β-values of the single CpGs within a region g (β-by-DMR) by group; Q3 and Q1 are third and first quartiles, respectively.

This procedure yielded a set G_{BC}, including 1778 hypermethylated and 6703 hypomethylated BC-specific DMR (Additional File 1: Table S4).

Details and characterization of the selected DMR are provided in Additional File 2: Supplementary Text and Fig. S1A-F.

Selection of ER status-informative DMR

ER status-informative DMR were identified from the previously defined BC-specific DMR by comparing CpG β-values from WGBS of ER+/HER2- (N = 24) and ER-/HER2- (N = 5) tumors in the BASIS dataset [39].

Let $g = 1, \ldots, B$ index the BC-specific DMR in G_{BC}. We select those satisfying the following criteria:

$$\left|\overline{\beta}_{\mathrm{ER+}}(g) - \overline{\beta}_{\mathrm{ER\text{-}}}(g)\right| > 0.2$$

where $\overline{\beta}(g)$ denotes the mean β-by-DMR values by group.

This procedure yielded 635 hypermethylated and 970 hypomethylated (ER+/HER2- vs. ER-/HER2- direction) DMR (Additional File 2: Supplementary Text and Fig. S1G–K).

The METER computational tool

METER is a computational tool to analyze ctDNA exploiting DMS and DMR from lpWGBS data of cfDNA samples. It comprises three modules: (1) METER-quant, to measure ctDNA level (i.e. TC), based on tumor-specific DMS; (2) METER-detect, to classify samples as ctDNA+ or ctDNA- (that is ctDNA is detected or not), based on tumor-specific DMR; (3) METER-subtype to infer specific subtype from ctDNA, based on tumor subtype-specific DMR.

METER-quant

METER-quant computes for a sample the proportion of tumor-like CpG sites (pTS) from lpWGBS data as a proxy for the sample's TC.

The α-value of a read is defined as the average methylation state across all CpGs covered by that read [42]:

$$\alpha(r) = \frac{1}{n_r}\sum_{i=1}^{n_r} x_{i,r}$$

where n_r is the number of CpGs covered by read r, and $x_{i,r} \in \{0, 1\}$ is the methylation call at CpG i in r ($1 = \mathrm{methylated}$, $0 = \mathrm{unmethylated}$).

For a sample j, we define $\mathrm{pTS}^{(j)}$ as the ratio between hypermethylated DMS with $\beta^{(j)}(s) = 1$ or hypomethylated DMS with $\beta^{(j)}(s) = 0$ (i.e., DMS consistent with the tumor-specific direction) and the total number of covered DMS with $\beta^{(j)}(s) \in \{0, 1\}$. To reduce bisulfite-conversion artifacts and increase specificity, $\beta^{(j)}(s)$ is computed considering only reads with $\alpha(r) \in \{0, 1\}$ and $n_r \geq 6$ (user selectable parameter). Formally, let

$$\begin{array}{l} s = 1, \ldots, S \text{ index the DMS;} \\ D^{(j)} = \left\{ s : \beta^{(j)}(s) \in \{0,1\} \right\}; \end{array}$$

$T(s) \in \{\mathrm{hyper},\mathrm{hypo}\}$ (tumor versus normal direction).

We define:

$$\tau^{(j)}(s) = \begin{cases} 1 \text{ if } T(s) = \mathrm{hyper} \text{ AND } \beta^{(j)}(s) = 1 \\ 1 \text{ if } T(s) = \mathrm{hypo} \text{ AND } \beta^{(j)}(s) = 0 \\ 0 \text{ otherwise} \end{cases},$$

$$\mathrm{pTS}^{(\mathrm{j})} = \frac{\sum_{\mathrm{s}\in \mathrm{D}^{(\mathrm{j})}} \tau^{(\mathrm{j})}(\mathrm{s})}{|\mathrm{D}^{(\mathrm{j})}|}$$

where $\beta^{(\mathrm{j})}(\mathrm{s})$ is computed considering only reads with $\alpha(\mathrm{r}) \in \{0,1\}$ and $\mathrm{n_r} \geq 6$.

In addition to the direct TC estimate through pTS, we trained a linear model on 94 (60%) randomly selected samples (N = 76 tumors, N = 18 controls) from the MIMESIS-1 cohort, using pTS as predictor and reference TC given by 0 for control cfDNA and ichorCNA-estimated [16] TC for tumor cfDNA. The model was then evaluated on the remaining 60 (40%) samples (N = 48 tumors, N = 12 controls), and negative predictions were truncated to zero. Parameters and results are shown in Additional File 2: Fig. S2 and Additional File 1: Table S5.

METER-detect

METER-detect computes for a sample the proportion of tumor-like sequencing reads (pTR) from lpWGBS, and then classifies the sample as ctDNA-positive (ctDNA+, METER+) or ctDNA-negative (ctDNA–, METER–) through a Z-score rule relative to the distribution in control cfDNA samples (reference distribution).

As in METER-quant, we retain reads with $\alpha(\mathrm{r}) \in \{0, 1\}$ and $\mathrm{n_r} \geq 6$ (user selectable parameter), and define $\mathrm{pTR}^{(\mathrm{j})}$ as the ratio between retained reads with $\alpha(\mathrm{r}) = 1$ mapping to hypermethylated DMR or reads with $\alpha(\mathrm{r}) = 0$ mapping to hypomethylated DMR (i.e., reads consistent with the tumor-specific direction) and the total number of retained reads. Formally, let

$$\mathrm{g} = 1, \ldots, \mathrm{G} \text{ index the DMR;}$$

$$\mathrm{T}(\mathrm{g}) \in \{\text{hyper, hypo}\} \text{ (tumor versus normal direction);}$$

$$\mathrm{R}^{(\mathrm{j})} = \{\mathrm{r} : \alpha(\mathrm{r}) \in \{0,1\} \text{ AND r maps to some } \mathrm{g} \in \mathrm{G}\}.$$

We define:

$$\tau^{(\mathrm{j})}(\mathrm{r}) = \begin{cases} 1 \text{ if } \mathrm{T}(\mathrm{g}) = \text{hyper AND } \alpha(\mathrm{r}) = 1 \\ 1 \text{ if } \mathrm{T}(\mathrm{g}) = \text{hypo AND } \alpha(\mathrm{r}) = 0 \\ 0 \text{ otherwise} \end{cases},$$

$$\mathrm{pTR}^{(\mathrm{j})} = \frac{\sum_{\mathrm{r}\in \mathrm{R}^{(\mathrm{j})}} \tau^{(\mathrm{j})}(\mathrm{r})}{|\mathrm{R}^{(\mathrm{j})}|}.$$

Then, for a sample j, we compute the Z-score relative to controls:

$$\mathrm{Z}^{(\mathrm{j})} = \frac{\mathrm{pTR}^{(\mathrm{j})} - \mu_{\mathrm{ctrl}}}{\sigma_{\mathrm{ctrl}}}$$

where μ_{ctrl} and σ_{ctrl} denote, respectively, the mean and standard deviation of pTR across control cfDNA samples.

Finally, for a sample j

$$\mathrm{j} = \begin{cases} \mathrm{ctDNA+} & \text{if } \mathrm{Z}^{(\mathrm{j})} > \mathrm{z_t} \\ \mathrm{ctDNA-} & \text{if } \mathrm{Z}^{(\mathrm{j})} \leq \mathrm{z_t} \end{cases}.$$

Where $\mathrm{z_t}$ is a user selectable threshold, and for this study $\mathrm{z_t} = 3$ (precomputed thresholds corresponding to Z-scores of 2, 3, and 4 relative to the 30 controls from the MIMESIS-1, are provided in METER-detect).

Prior to pTR computation, an additional filter was applied to exclude DMR exhibiting unexpected methylation signal in control samples. Specifically:

- any hypermethylated DMR that was covered by one or more reads with $\alpha(\mathrm{r}) = 1$ and $\mathrm{n_r} \geq 6$ (i.e. exhibiting an unexpected tumor-like methylation pattern) in at least three control samples was excluded.
- any hypomethylated DMR that was covered by one or more reads with $\alpha(\mathrm{r}) = 0$ and $\mathrm{n_r} \geq 6$ in at least three control samples was excluded.

For the 30 samples considered in this study, a total of 40 DMR were excluded (Additional File 1: Table S6).

METER-subtype

METER-subtype was developed to infer tumor subtype from cfDNA samples using selected subtype-specific DMR and the EpiDISH R package [43], which implements reference-based deconvolution via robust partial correlations (RPC). While the original application of EpiDISH exploited β-values of informative CpGs, we reasoned that in low-pass settings, leveraging β-values of informative DMR, taking advantage of the pervasive nature of DNA methylation, would provide greater granularity.

To assess ER status from lpWGBS of the MIMESIS-1 and MIMESIS-2 cfDNA samples, we selected 1605 ER status-informative DMR (Additional File 2: Supplementary Text and Additional File 1: Table S7 for the genomic coordinates of selected DMR) and built a three-component reference model (ER+, ER-, healthy cfDNA). Reference profiles were obtained as median β-by-DMR values, defined as the mean β-values of CpGs within each DMR, using ER+/HER2- and ER-/HER2- samples from the BASIS dataset [39], and healthy cfDNA samples from Loyfer et al. [40]. For lpWGBS cfDNA data, β-by-DMR values were computed as the ratio of methylated to total calls across all CpGs within each DMR, and used to estimate ER+ and ER- weights. ER status was then assigned according to the maximum weight between ER+ and ER-.

This procedure was integrated into METER-subtype module and generalized to support custom subtype definitions and marker sets.

Analysis of false discovery rate of METER-detect

The false discovery rate (FDR) of METER-detect was assessed through a leave-one-out strategy applied to pTR in control samples. At each iteration, one control sample was classified as METER+ or METER- based on the reference model (mean and sd for Z-score and DMR cleaning) estimated using the other 29 samples. The relationship between FDR and Z-score thresholds, from 1 to 6, was investigated. Following this procedure, we classified 0 out of 30 controls as ctDNA+ using a Z-score = 3, supporting an FDR of less than or equal to 0.05 in our dataset.

Copy number alterations-based estimation of tumor content in cfDNA using ichorCNA

To quantify and detect ctDNA based on copy number alterations (CNAs), ichorCNA version 0.3.2 [16] was applied to lpWGBS data from cfDNA samples in the MIMESIS-1 and MIMESIS-2 cohorts. To evaluate the feasibility of applying ichorCNA to WGBS, we first evaluated its reliability using nine cfDNA samples from advanced metastatic prostate cancer patients with matched WES and WGBS [10] (Additional File 2: Supplementary Text and Fig. S3 and S4), demonstrating excellent concordance for CNA profiling and consistent TC estimates, in line with previous studies [20, 44, 45]. For the analysis on lpWGBS data, we included only reads with a mapping quality ≥ 20, used a genomic bin size of 500 kb, setting a normal fraction range from 0 to 0.99. A reference panel of normal samples was generated using lpWGBS data from 30 healthy cfDNA samples from the MIMESIS-1 dataset, using the dedicated ichorCNA R script. Samples were classified as ctDNA-positive (ichorCNA+) or ctDNA-negative (ichorCNA-) based on ichorCNA's lower detection limit of 3% tumor content.

Comparative analysis of METER with CancerDetector, CfDeconvolve and Griffin

We performed comparative analysis of METER-quant and METER-detect with CancerDetector [42] and METER-subtype with cfDeconvolve [42] and Griffin [23] in the MIMESIS-1 dataset. CancerDetector was applied via the cfTools R package version 1.8.0. Since the package does not provide predefined BC-specific reference model, we used our previously selected BC-specific DMR as input markers. CancerDetector was evaluated across a range of lambda values (representing the expected relative tumor burden) from 0.001 to 0.9, observing consistent and stable estimations starting at lambda = 0.4; therefore, the default lambda value (lambda = 0.5) was used for downstream analyses and comparison with METER. cfDeconvolve was applied using the cfTools R package version 1.8.0, using our predefined list of subtype-specific DMR, comprising three components (ER+/HER2-, ER-/HER2-, and healthy cfDNA). cfDeconvolve was evaluated using the two deconvolution algorithms available within the package, which produced highly concordant estimates of subtype contributions (Pearson's $R > 0.99$). Using the *em.global.unknown* algorithm, we computed the difference between ER+/HER2- and ER-/HER2- component estimates to construct a ROC curve to evaluate classification performance, using IHC biopsy as the reference standard. Griffin version 0.2.0 (https://github.com/adoebley/Griffin) was evaluated using the ER-differential ATAC-seq sites provided in the supplementary materials of the original publication and the pretrained model available at https://github.com/adoebley/Griffin_analyses/tree/main/final_models/ER_status. Classification performance was evaluated by generating a ROC curve based on the ER+ probability estimated by the model, using IHC biopsy as the reference standard.

Evaluation of coverage levels on METER-detect sensitivity

To evaluate the impact of coverage on detection sensitivity and FDR, in silico artificial dilutions at increasing coverage levels were generated (see section In vitro and in silico artificial samples). To account for the reduced variability of DNA methylation signals in these artificial control samples compared to real healthy cfDNA samples, we estimated the mean and standard deviation for calculating Z-scores at each coverage level using the 10 artificial controls that were not included in generating the dilutions.

Statistical analysis

Statistical analyses were performed with the R software environment for statistical computing and graphics (RCore team, 2022 https://www.R-project.org/). Survival analyses used the Cox proportional hazard method, with the log-rank test. OS was computed from the date of informed consent to death from any cause, PFS was computed from informed consent to disease progression or death. A multivariate Cox regression model was fitted to evaluate the independent effect of each covariate on OS and PFS. Relevant covariates were selected according to clinical relevance. These include: the number of treatment lines received for metastatic disease (no previous treatment vs. 1 or more lines) and the number of metastatic anatomic sites (single site vs. multiple sites). Mann-Whitney test was used to assess the significance of the relationship between continuous and categorical variables. Associations between continuous variables were evaluated using Pearson's or Spearman's correlation coefficients, as appropriate. Associations between categorical

variables were assessed using Fisher's exact test or Chi-squared test.

Results

Development of METER for the analysis of low-pass plasma methylome

In order to address a clinically challenging tumor-content range, we conducted our study on two independent datasets derived from early-line treatment mBC cohorts: MIMESIS-1 [27] (qualification cohort, comprising 154 plasma samples from 30 healthy donors and 59 mBC patients; Fig. 1A left and Additional File 1: Table S1) and MIMESIS-2 (validation cohort, comprising 214 plasma samples from 65 mBC patients; Fig. 1A right and Additional File 1: Table S2). MIMESIS-1 included plasma collection at baseline (BL), after cycle 1 treatment (C2D1), and at progression (Prog). MIMESIS-2 expanded this design by including additional serial plasma samples collected at the first three imaging evaluations (I1–I3). lpWGBS was performed on all cfDNA samples, with full details reported in the Methods and summarized in Fig. 1A.

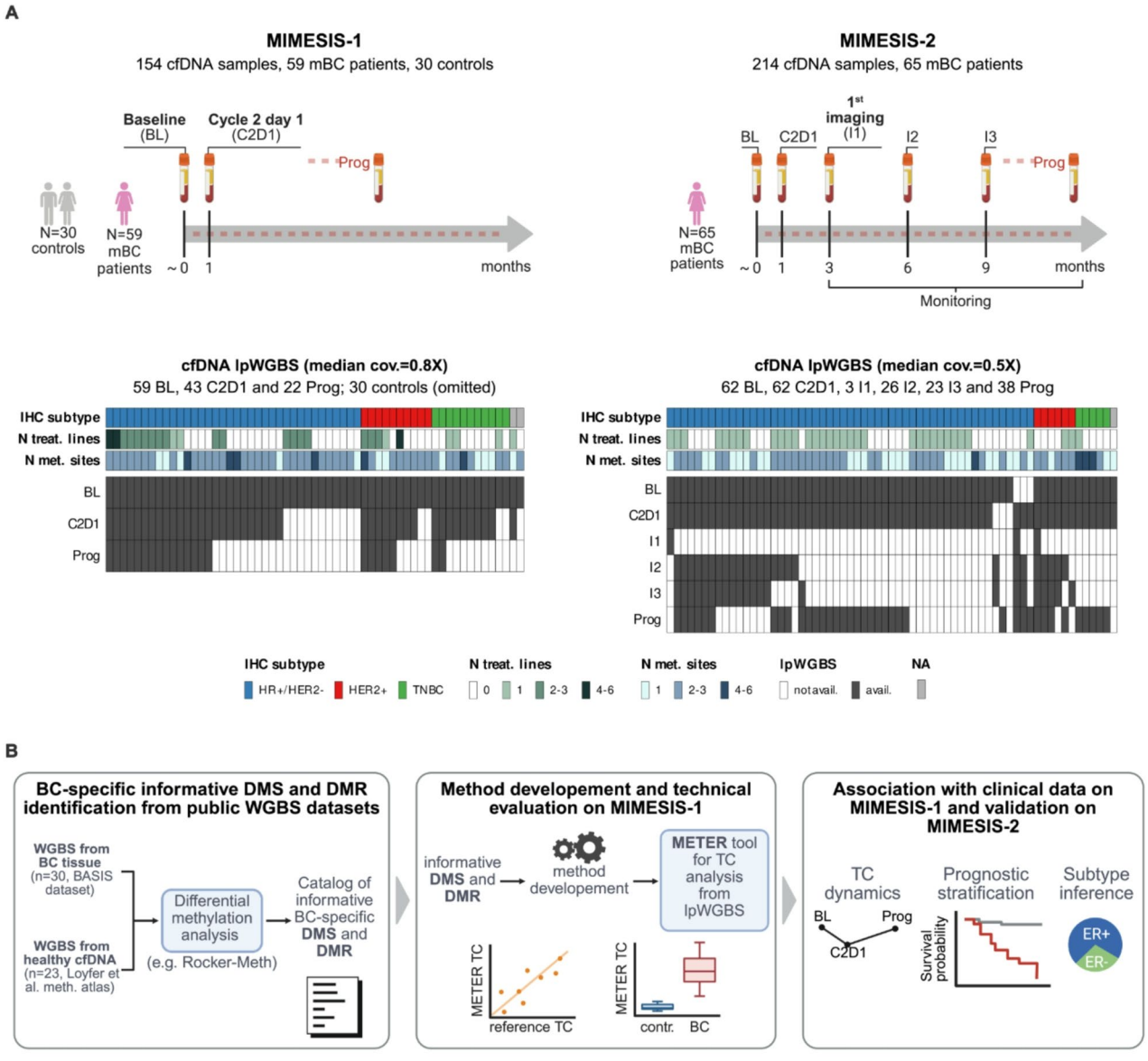

Fig. 1 The MIMESIS-1 and the MIMESIS-2 study cohorts and overview of the study. **A** Schematic of the MIMESIS-1 (top left panel) and MIMESIS-2 (top-right panel) studies. Heatmaps showing profiled mBC plasma samples from the MIMESIS-1 (bottom left panel) and MIMESIS-2 (bottom right panel) study cohorts, comprising 124 samples from 59 mBC patients and 214 samples from 65 mBC patients, respectively. For each patient, the availability of samples at different time points along with relevant clinical characteristics is reported. **B** Overview of the study, illustrating: identification of differentially methylated sites (DMS) and differentially methylated regions (DMR) by differential methylation analysis on public datasets; METER tool development and technical evaluation on the MIMESIS-1 dataset; evaluation of METER's clinical relevance on the MIMESIS-1 and validation of results on the MIMESIS-2

The primary aim of this study was to develop a practical and cost-effective strategy for ctDNA detection, quantification, and molecular profiling, with potential for routine clinical implementation in metastatic settings, including early-line treatment. We reasoned that DNA methylation holds instrumental features to our goal: cancer-related DNA methylation patterns are genomically pervasive and prevalent across tumor types, offering a robust signal, suitable for shallow genome-wide sequencing. Moreover, as DNA methylation encodes cell identity and transcriptional programs, it can potentially reveal tumor-specific transcriptional states, enabling inference of tumor subtype from ctDNA.

Based on these considerations, we developed the METER computational workflow for plasma low-pass methylome analysis, leveraging tumor-specific differentially methylated CpG sites (DMS) and regions (DMR), pre-computed from independent WGBS data [39, 40] (Fig. 1B left box; Methods). Details and characterization of the selected DMR are provided in Additional File 2: Supplementary Text and Fig. S1. METER is composed of three modules: (i) METER-quant, to measure TC in cfDNA, (ii) METER-detect, to detect ctDNA in cfDNA classifying samples as ctDNA+/-, and (iii) METER-subtype, to infer molecular subtype from cfDNA (Methods). To evaluate METER's performance, we generated reference TC estimates through ichorCNA [16] and assessed the clinical relevance of its predictions, exploiting curated clinical data and CTC counts from the MIMESIS-1 study. Results were then validated in the MIMESIS-2 dataset to test METER's reliability as a tool for the monitoring of patients on first- or second- line treatment for mBC (Fig. 1B middle and right boxes).

METER-quant provides precise TC quantification

METER-quant was developed to achieve accurate TC quantification from plasma cfDNA low-pass methylomes. It provides TC estimates by evaluating the methylation status of prevalent tumor-type-specific DMS and computing the proportion of tumor-like CpG sites (pTS) (Fig. 2A and Methods). To evaluate the performance of METER-quant, we applied it to 154 plasma samples of the MIMESIS-1 dataset, using about 200,000 previously selected BC-specific DMS (Additional File 1: Table S3). In tumor samples, TC ranged between 0 and 52%, statistically significantly higher (p < 1e-10) than TC values in controls (Fig. 2B left, data reported in Additional File 1: Table S8). We then compared METER-quant estimates with those from ichorCNA [16]. The TC values for the 124 cfDNA mBC samples estimated by METER-quant were highly concordant with those obtained from the state-of-the-art tool ichorCNA (R > 0.90, p < 1e-50) (Fig. 2B right). METER-quant showed accurate and comparable estimation also for low TC values, in the range of 3%–10% as estimated by ichorCNA. For lower values, we observed poor concordance (R = 0.27, p = 0.04), as expected based on ichorCNA's lower detection limit of 3% TC. To examine the ability of METER-quant to provide accurate measures for low-level TC, we generated artificial samples consisting of serial dilutions (0%, 0.1%, 0.5%, 1%, 2.5%, 5%) of DNA from luminal T47D BC cell line culture medium, as a surrogate of ctDNA, with commercial human genomic DNA from white blood cells (Fig. 2C). As expected, we observed that ichorCNA loses linearity in predicting TC (median absolute error, MAE = 0.01, root mean square error RMSE = 0.01), still maintaining high correlation (R = 0.95, rho = 0.86) with expected values. On the other hand, METER-quant showed accurate estimation down to 0.5–1%, obtaining higher correlation with expected values (R = 0.96, rho = 0.95) and lower dispersion (MAE = 0.005, RMSE = 0.006) than ichorCNA (Fig. 2C and Additional File 1: Table S9). We finally tested whether using a model for training METER-quant could enhance the accuracy of TC estimations. We developed a linear model using 60% of lpWGBS samples from our study cohort as a training set (N = 94, including 18 controls and 76 tumors), while the remaining 40% (N = 60) served as a test set (model parameters reported in Additional File 1: Table S5). pTS was used as the predictor variable, and observed values were used as references (ichorCNA TC estimates for tumor samples and 0% TC for control samples). Within the test set, control samples exhibited a median TC of 0% (range 0–1%), whereas tumor samples had a significantly higher median TC of 4% (range 0–60%) compared to controls (p < 1e-5) and a strong concordance between observed and predicted values within the test set (R = 0.94, p < 1e-28) was obtained (Additional File 2: Fig. S2).

METER-detect enables sensitive detection of low ctDNA levels

METER-detect was developed to detect the presence of ctDNA in low TC settings. It leverages tumor-type-specific informative DMR to classify cfDNA samples based on the presence (ctDNA+ or METER+) or absence (ctDNA- or METER-) of ctDNA. Briefly, evaluating the methylation status of reads mapping to informative DMR, METER-detect computes the proportion of tumor-like reads (pTR) and uses a Z-score method to classify samples as ctDNA+/- based on pTR distribution in controls (Fig. 2D and Methods). We applied METER-detect to control and tumor cfDNA samples from the MIMESIS-1, using about 8,000 previously selected BC-specific DMR (Additional File 1: Table S4, S8). To specifically test METER-detect's performance in low TC ranges, we focused on 60 tumor samples that scored below ichorCNA [16] lower limit of detection (3%), thus undetected by ichorCNA (ichorCNA-). As expected, we

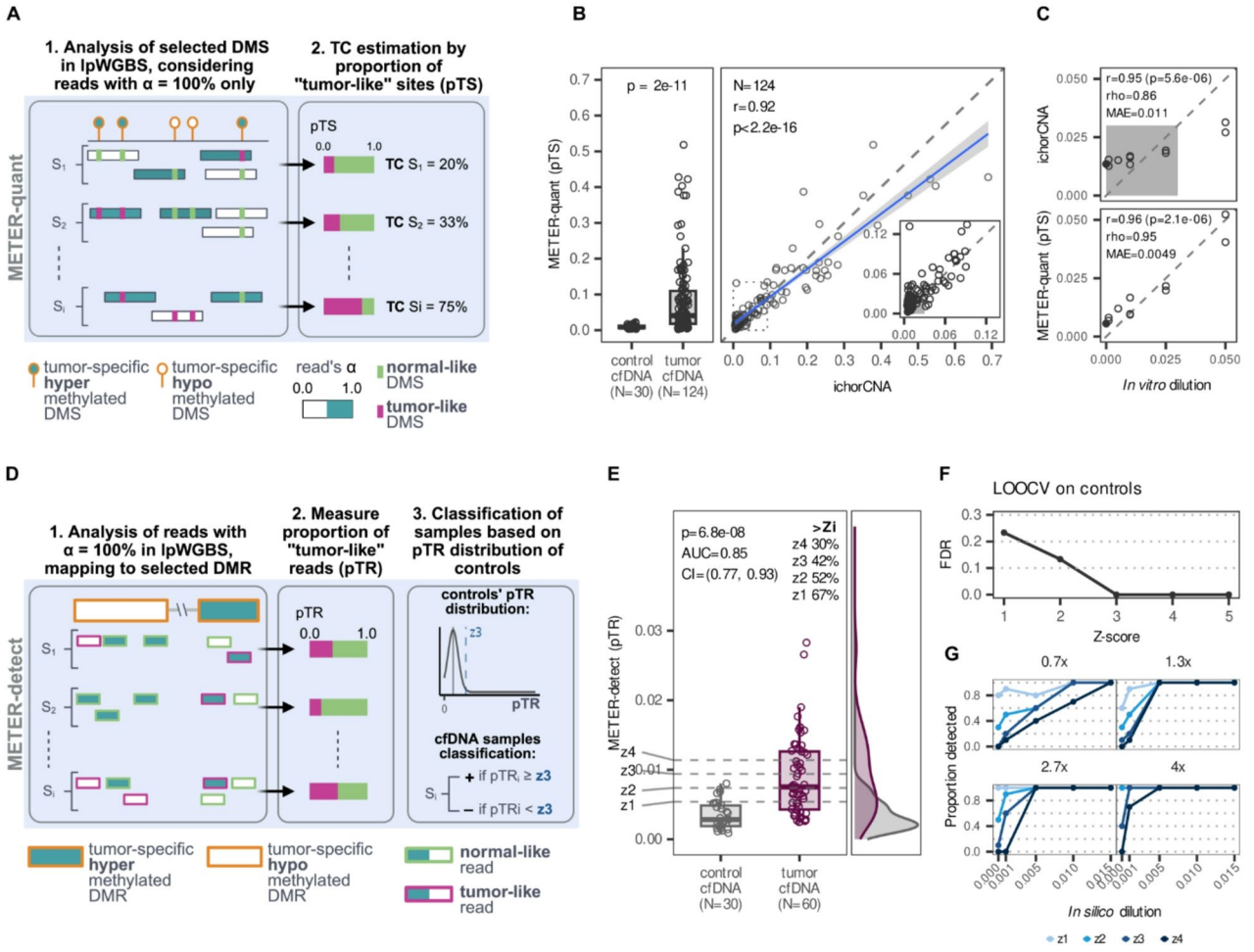

Fig. 2 TC quantification by METER-quant and ctDNA detection by METER-detect on cfDNA samples from the MIMESIS-1 cohort. **A** Overview of METER-quant: METER-quant evaluates the methylation status of tumor-type-specific DMS, identified from independent public datasets, and computes the proportion of tumor-like CpG sites (pTS) to estimate TC from low-pass whole methylome of cfDNA samples. **B** Box plots showing the distribution of TC estimates by METER-quant in control and mBC cfDNA samples from the MIMESIS-1 cohort. p value is from the Wilcoxon test. (left panel). Scatter plot showing TC estimates of mBC cfDNA samples by METER-quant (y-axis) and ichorCNA [16] (x-axis). The inset plot reports samples with TC ranging in 0–10% according to ichorCNA. The shaded region highlights the range of TC where ichorCNA is not applicable (0–3%). r and p are Pearson's correlation coefficient and corresponding p-value, respectively (right panel). **C** Scatter plots of TC by ichorCNA (top panel) and METER-quant (bottom panel) versus in vitro serial dilutions of DNA from T47D BC cell line culture medium with commercial human genomic DNA from white blood cells. The filled dot represents the 0% TC dilution. The shaded region refers to the range of TC where ichorCNA is not applicable (0–3%). r and p are Pearson's correlation coefficient and corresponding p-value, rho is Spearman's correlation coefficient, MAE is mean absolute error. **D** Overview of METER-detect module: METER-detect evaluates the methylation status of reads mapping to tumor-type-specific DMR, selected from independent public datasets, and computes the proportion of tumor-like reads (pTR) for each sample. It classifies cfDNA samples as ctDNA+/-, using a Z-score threshold established from pTR distribution in controls. **E** Box plots and density plots showing the distribution of pTR by METER-detect in 30 control and 60 mBC cfDNA samples from the MIMESIS-1 cohort with TC by ichorCNA < 3% (ichorCNA-undetected samples). The dashed lines indicate different Z-score thresholds based on the distribution of pTR in controls, and percentages of tumor samples with Z-scores exceeding Z-score thresholds (Zi) are shown. Wilcoxon rank-sum test p-value and the area under the ROC curve (AUC) with corresponding 95% confidence interval (CI) are reported. Z-score = 3 corresponds to the threshold used in this study. **F** Leave-one-out-cross-validation study on control cfDNA samples to estimate FDR of METER-detect at different Z-score thresholds. **G** Line plots showing in silico dilutions generated to evaluate detection sensitivity and FDR of METER-detect at increasing mean coverage levels (indicated above each plot) and Z-score thresholds

observed no statistically significant difference between ichorCNA TC estimates of ichorCNA- versus control samples (p = 0.06, AUC = 0.62) (Additional File 2: Fig. S5). On the contrary, pTR measured by METER-detect showed significantly different levels between tumor and control samples (p < 1e-7, AUC = 0.85, 95% CI: 0.77–0.93) (Fig. 2E). Using the pTR value corresponding to a Z-score of 3, METER-detect reclassified 42% (25 out of 60 samples) of ichorCNA- samples as METER+. Performing a leave-one-out-cross-validation (LOOCV) procedure on control samples, we evaluated FDR at different

thresholds of Z-score, obtaining FDR < 5% for Z-score = 3 (Fig. 2F).

We then performed a comparative analysis between METER and CancerDetector [42], a ctDNA detection method that operates on plasma whole-methylome data to detect low ctDNA levels at low-to-moderate sequencing coverage (Additional File 2: Fig. S6). In tumor samples, we observed that TC estimates from CancerDetector positively correlate with estimates from ichorCNA (R = 0.86) and METER-quant (R = 0.91), although with inaccurate slopes. We next compared TC by CancerDetector with the pTR metric used by METER-detect, focusing on tumor samples undetected by ichorCNA (TC < 3%). pTR by METER-detect demonstrated a stronger differential signal between tumor and control samples (Fig. 2E) compared to CancerDetector (p < 0.01, AUC = 0.67, 95% CI: 0.55–0.8), indicating higher sensitivity and specificity. We further used CancerDetector to assess the reliability of METER-detect calls. Of note, CancerDetector TC in METER positive samples resulted in significantly higher levels than in both controls (p = 3.8e-05) and METER negative samples (p = 7e-06).

To preliminarily assess the potential of METER to detect ctDNA in early-stage disease, we analyzed plasma samples collected prior to surgery from a few primary colorectal cancer (CRC) patients, enrolled in the LIBIMET study [32]. Using a list of CRC-specific DMR (Additional File 2: Supplementary Text), we observed significantly higher levels of pTR in tumor samples compared to controls (p < 0.01, AUC = 0.89, 95% CI: 0.77–1) (Additional File 2: Fig. S7).

In silico evaluation of coverage on METER-detect performance

We then conducted extensive in silico studies to evaluate the performance of our method based on the coverage of plasma methylomes. Considering 10 in silico dilutions at TC = 0, corresponding to 10 different pools of lpWGBS data of plasma samples from healthy donors, at each coverage level, we observed a decrease in FDR with an increase in the Z-score threshold, as expected. Within the coverage range of this study (0.2-1X) and with Z = 3, we observed an FDR of less than 10%, consistent with the LOOCV study performed on real samples. The analysis also indicated a sensitivity of 100% and 60% for TC 1% and 0.5%, respectively. Notably, this synthetic study indicates that the sensitivity of METER-detect may increase with the coverage level, suggesting the possibility of detecting ctDNA at TC = 0.1% with a sensitivity of 70% using Z = 4 in WGBS 4x, while maintaining an FDR of less than 10% (Fig. 2G).

METER predictions associate with relevant clinical prognostic factors

To assess the potential clinical applicability of METER, we examined the results obtained in MIMESIS-1 with relevant patients' clinical data. We observed a positive correlation between METER-quant TC at BL and the number of metastatic sites at study entry, a proxy of tumor burden (Spearman's rho = 0.44, p < 1e-3) (Fig. 3A), and higher although not significant TC values were observed in patients with visceral disease vs. bone or non-visceral (p = 0.08) (Additional File 2: Fig. S8A-B). Interestingly, we did not observe a trend indicating an increase in TC for later treatment lines (Additional File 2: Fig. S8C). METER-quant revealed expected TC modulation across serial time points. In 43 patients having matched pre-treatment BL and C2D1 plasma samples, a significant drop of TC at C2D1 was observed (paired p < 1e-4), confirming the expected sensitivity to treatment for most of the patients. Moreover, the 22 patients with matched C2D1-Prog samples exhibited a significant TC increase at disease progression as expected (p < 0.04) (Fig. 3B). Coherent results at serial time points were provided by METER-detect classification (Additional File 2: Fig. S8D-F). Overall, comparable results were obtained performing these analyses with ichorCNA [16], although less or not significant associations were observed in some cases (Additional File 2: Fig. S9A-H).

METER-detect provides relevant prognostic stratification of patients with TC levels below 3%

To further qualify its clinical relevance, we tested METER-detect ability to provide effective prognostic stratification of patients by its association with progression-free survival (PFS) and overall survival (OS) in the MIMESIS-1. We first stratified patients based on ctDNA detection at BL provided by METER-detect (METER+ or METER-) or ichorCNA [16] (ichorCNA+ if TC by ichorCNA ≥ 3%, ichorCNA- otherwise). METER-detect identified 46 out of 59 patients as ctDNA+, while ichorCNA classified as ctDNA+ 36 out of 59 patients. METER+ patients at BL showed a statistically significant shorter PFS (hazard ratio (HR) = 3.8, 95% p < 0.001) compared to METER-, while no significant association was obtained using stratification provided by ichorCNA. Limiting the analysis to ichorCNA- patients, significantly worse PFS for METER+ patients compared to METER- was observed (HR = 3.9, CI = 1.5–10.0, p = 0.003) despite the small number (n = 23) (Fig. 3C). Results were confirmed using OS, where ichorCNA also demonstrated significant patients' stratification (Additional File 2: Fig. S10A-D). We then examined the dynamic changes in ctDNA detection from BL to C2D1 (BL/C2D1) for the 43 patients, with samples available for both time points. Overall, METER-detect classified 18 patients as +/+,

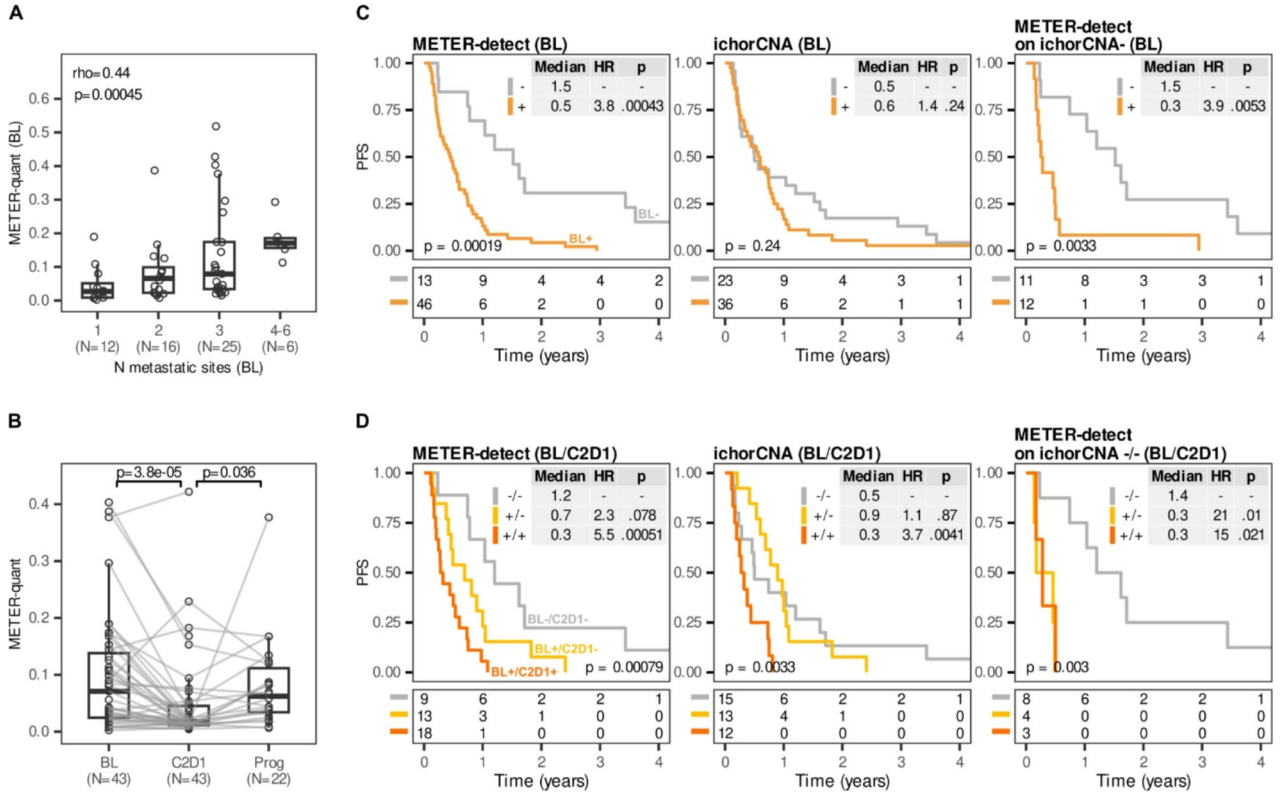

Fig. 3 Association of METER predictions with relevant clinical factors and patients' outcome from the MIMESIS-1 cohort. **A** Box plots showing the distribution of TC, as quantified by METER-quant (y-axis), in mBC samples at BL, stratified by the number of metastatic sites at study entry; rho is Spearman's correlation coefficient; p value is from Pearson's correlation test. **B** Box plots showing the distribution of samples'TC, as quantified by METER-quant (y-axis), across clinical time points (x-axis) in mBC patients from the MIMESIS-1 cohort with matched BL-C2D1 and C2D1-Prog samples. p values are from paired Wilcoxon test. **C** Kaplan-Meier curves showing PFS of patients from the MIMESIS-1, stratified according to ctDNA detection (+ or -) at BL by METER-detect and ichorCNA [16]. The left and middle panels include all patients with BL samples, while the right panel includes only ichorCNA- patients at BL, stratified according to METER-detect. p values shown in Kaplan-Meier curves are from the Log-Rank test. **D** Kaplan-Meier curves showing PFS of patients from the MIMESIS-1 study, stratified by ctDNA detection at BL and C2D1 (-/-, +/-, or +/+) by METER-detect and ichorCNA. The left and middle panels include all patients with matched BL and C2D1 time points, while the right panel includes only ichorCNA-/- patients at both time points, stratified according to METER-detect. p values shown in Kaplan-Meier curves are from the Log-Rank test

13 as +/-, 2 as -/+ and 9 as -/-, while ichorCNA classified 12 patients as +/+, 13 as +/-, 2 as -/+ and 15 as -/-. Patients classified as -/+ by METER or ichorCNA (n = 3, 1 identified by both METER-detect and ichorCNA) were excluded due to low sample size (results for all patients are reported in Additional File 2: Fig. S11 A–B). Considering PFS, METER-detect demonstrated again superior prognostic stratification of patients ($p < 0.001$) compared to ichorCNA ($p = 0.003$), especially due to its more reliable identification of ctDNA-/- patients (median PFS of 1.2 years and 0.5 years for METER-detect and ichorCNA, respectively). Remarkably, even among the 15 patients classified as -/- by ichorCNA, METER-detect still achieved a significant stratification ($p = 0.003$) (Fig. 3D). The superior prognostic performance of METER was further qualified using OS (Additional File 2: Fig. S11B). Notably, associations with PFS and OS remained significant even after adjusting for clinically relevant covariates (Additional File 1: Table S10). Patients' classification concordance by ichorCNA and METER-detect is reported in Additional File 2: Fig. S12A–D.

METER associates with independently assessed circulating tumor cells data and provides enhanced prognostic stratification

Of the 124 samples in the MIMESIS-1, 121 had existing CTC data [29–31], allowing us to investigate the association with this clinically established and independent liquid biopsy biomarker. We observed a positive correlation between TC estimates from both METER-quant (rho = 0.57, $p <$ 1e-11; Additional File 2: Fig. S13A) and ichorCNA [16] (rho = 0.57, $p <$ 1e-10; Additional File 2: Fig. S13B) with CTC counts. METER+ samples showed significantly higher CTC counts compared to METER-, particularly in ichorCNA- cases ($p = 0.002$), further confirming METER-detect reliability below 3% of TC (Fig. 4A). In detail, only 8 out of 37 (22%) METER- samples showed CTC > 0, with a range of 1–3. We then used the

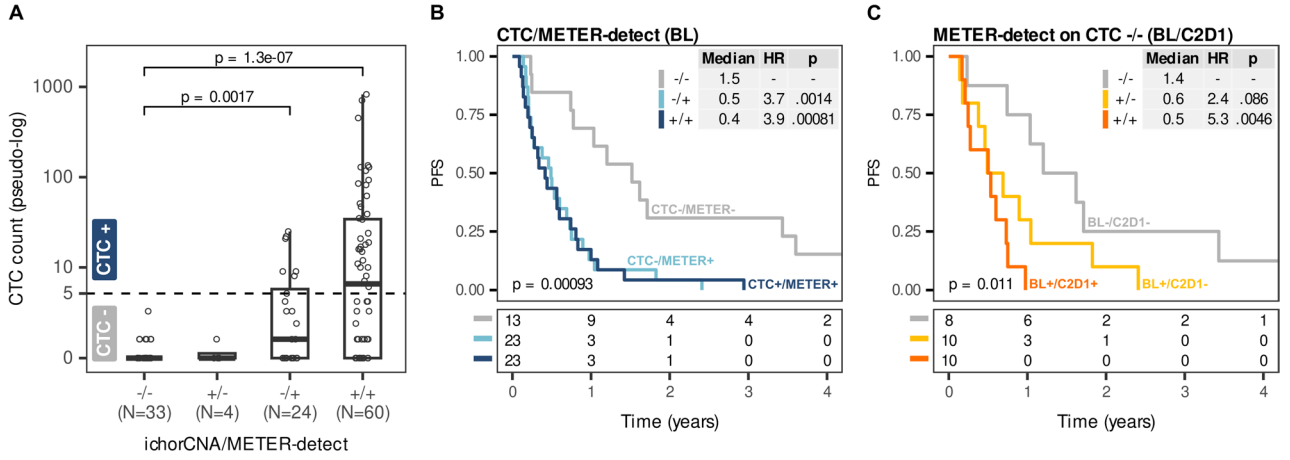

Fig. 4 Matched CTC and ctDNA detection data, and their association with patient outcome in the MIMESIS-1 cohort. **A** Box plots showing the distribution of the CTC counts (y-axis, pseudo-log scale) in plasma samples from the MIMESIS-1 study, stratified according to ctDNA detection by ichorCNA [16] and METER-detect (-/-, +/-, -/+ and +/+) from matched cfDNA samples. The dashed line indicates a CTC count of 5, the threshold used for CTC detection and classify samples as CTC-positive (CTC count ≥ 5, CTC+) or CTC-negative (CTC count < 5, CTC-). p values are from the Wilcoxon test. **B** Kaplan-Meier curves showing PFS of patients from the MIMESIS-1 study stratified based on combined CTC detection and ctDNA detection by METER-detect (-/-, -/+ and +/+) of BL samples. p values shown in Kaplan-Meier curves are from the Log-Rank test. **C** Kaplan-Meier curves showing PFS of patients from the MIMESIS-1 cohort, with CTC -/- status at both BL and C2D1, stratified by ctDNA detection at BL and C2D1 according to METER-detect (-/-, +/-, or +/+). p values shown in Kaplan-Meier curves are from the Log-Rank test

clinically validated threshold of 5 CTCs to classify samples as CTC+ (CTC- otherwise) [46, 47] (Fig. 4A and Additional File 2: Fig. S13C) and evaluated the outcome of patients stratifying them according to the combined CTC status and ctDNA detection by METER-detect in BL samples (Fig. 4B and Additional File 2: Fig. S13D). Notably, patients who were CTC- but METER+ at BL (-/+) had significantly worse PFS and OS compared to -/- patients (p = 0.001 and p < 1e-3, respectively), with outcomes comparable to +/+ patients. This analysis indicated METER superior prognostic capability compared to CTCs, further supporting the clinical validity of METER predictions. To further evaluate the reliability of METER-detect and its ability to provide prognostic information beyond that of CTCs, we analyzed ctDNA detection dynamics from BL to C2D1, as determined by METER-detect, in patients classified as CTC- at both time points. Despite the limited sample size, we observed significant stratification of outcomes for both PFS and OS. (Fig. 4C and Additional File 2: Fig. S13F).

METER-subtype accurately infers ER status in plasma samples from patients with metastatic breast cancer

In breast cancer, ER status may change during metastatic progression due to resistance to endocrine therapy and/or chemotherapy [48], and performing serial tissue biopsies is usually not feasible, especially in the case of brain metastases [49]. The ability to assess ER status non-invasively through ctDNA analysis is therefore becoming an increasingly important clinical need. To this end, we developed METER-subtype. Starting from the previously selected DMR, we identified a set of ER-status informative DMR through a comparative analysis between ER+/HER2- and ER-/HER2- BC from the BASIS WGBS dataset [39]. Then, we implemented a workflow, integrated into the METER-subtype module, exploiting these subtype-specific DMR to deconvolve the signal from low-pass methylome of cfDNA into ER+, ER- and normal cfDNA components through the robust partial correlation (RPC) method [43] (Fig. 5A and Methods). Subtype DMR exhibited distinctive patterns of DNA-methylation median levels in ER+/HER2- and ER-/HER2- reference samples, confirming the reliability of our selection procedure (Fig. 5B and Additional File 1: Table S7). Since our reference methylation model did not include HER2+ samples due to the low numerosity of this subtype in the BASIS dataset [39], we limited METER-subtype analysis to HER2- BC samples from the MIMESIS-1, considering available immunohistochemistry (IHC) on the most recent archived sample as BC subtype ground truth (Additional File 2: Fig. S14A–D and Additional File 1: Table S8). We first observed that in ER+/HER2- and ER-/HER2- samples defined by IHC, TC by METER-quant strongly correlated with ER+ and ER- RPC components respectively (R > 0.9, p < 1e-10 for both ER+ and ER-), while no significant association with TC was obtained for ER+ component in ER-/HER2- samples (R = 0.42, p = 0.054) and for ER- component in ER+/HER2- samples (R = 0, p = 1) (Additional File 2: Fig. S14A and S14B-C for the distribution of RPC components values). To evaluate the ability to assess ER status by using the difference between ER+ and ER- RPC components for each sample, we conducted a receiver operating characteristic (ROC) curve analysis on distinct sample

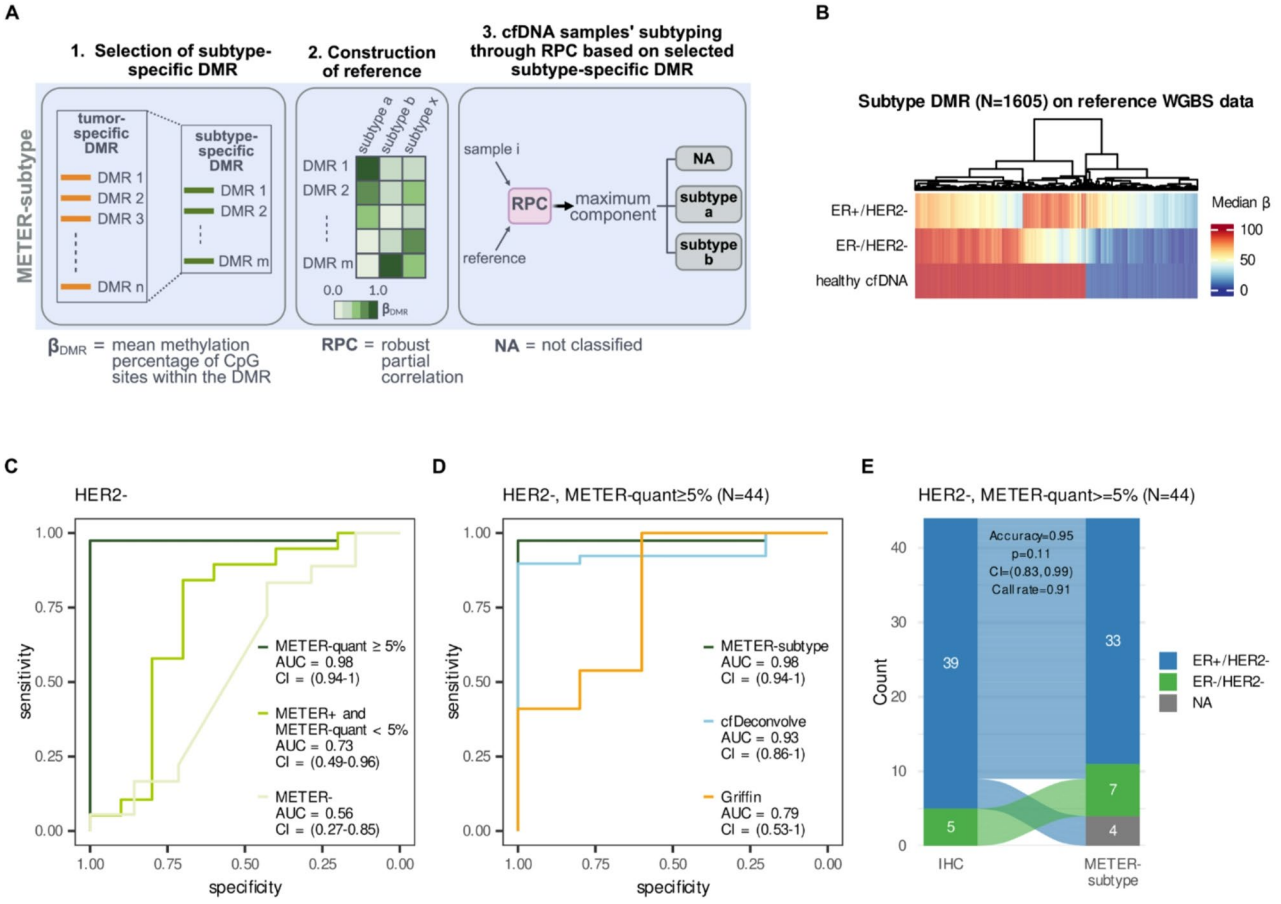

Fig. 5 ER subtyping by METER-subtype on cfDNA samples from the MIMESIS-1 cohort. **A** Overview of METER-subtype: METER-subtype infers tumor subtypes (ER+/HER2- or ER-/HER2- in this study) from cfDNA low-pass whole methylome data by analyzing subtype-specific DMR and deconvolving tumor signal using the RPC method implemented in the EpiDISH tool [43]. **B** Unsupervised clustering of selected subtype DMR based on median β by DMR in reference ER+/HER2- ($N = 24$) and ER-/HER2- ($N = 5$) from the BASIS cohort [39] and WGBS of healthy cfDNA ($N = 30$) from Loyfer et al. [40]. Clustering method: complete-linkage hierarchical clustering based on euclidean distance. **C** ROC curves illustrating METER-subtype classification performance based on the difference between ER+/HER2- and ER-/HER2- RPC components, at varying threshold values, considering IHC as reference subtype, for samples from the MIMESIS-1 in different TC ranges. **D** ROC curves of METER-subtype, cfDeconvolve [42], and Griffin [23] applied to HER2- samples from the MIMESIS-1 study with METER-quant ≥ 5%, using IHC as the reference subtype. **E** Alluvial plot showing concordance between ER status as assessed by IHC and by METER-subtype for samples with TC by METER-quant ≥ 5% from the MIMESIS-1. Reported p-value is estimated from a binomial test to evaluate whether the observed classification accuracy is significantly higher than would be expected by chance (no-information rate)

sets corresponding to different TC ranges. We achieved high classification performance (AUC = 0.98, 95% CI: 0.94–1) for samples with TC values of METER-quant ≥ 5%, while poor performance was observed for METER- as expected (AUC = 0.56, 95% CI: 0.27–0.85). Interestingly, our findings suggest the potential to infer ER status even in cases of low TC values, albeit with reduced accuracy, as demonstrated by METER+ samples with TC < 5% (AUC = 0.73, 95% CI: 0.49–0.96) (Fig. 5C and Additional File 2: Fig. S14B). We then compared the performance of METER-subtype with cfDeconvolve [42] and Griffin [23], on samples with TC ≥ 5% ($n = 44$). METER-subtype showed superior and comparable classification compared to Griffin (AUC = 0.79, CI = 0.53–1) and cfDeconvolve (AUC = 0.93, CI = 0.86–1) (Fig. 5D), respectively. Similar comparative results were obtained with TC ≥ 3% (Additional File 2: Fig. S14D) samples. ER status was then assigned based on the predominant component between ER+ and ER- and compared to IHC. Among the 44 samples with METER-quant ≥ 5%, METER-subtype showed a classification accuracy of 0.95 (95% CI: 0.83–0.99), with a call rate (CR) of 0.91, as in 9% of cases ($N = 4$) RPC was unable to estimate ER+ and ER- component's level. Statistical significance was however not reached ($p = 0.11$), likely due to the limited number of ER- samples (Fig. 5E).

METER predictions validate in the MIMESIS-2 study

After evaluating METER on the MIMESIS-1 dataset, we further evaluated its performance in plasma samples from the independent MIMESIS-2 study (Additional File 1: Table S11). We observed an excellent concordance between TC estimates by METER-quant and ichorCNA

[16] for the 214 cfDNA mBC samples available (Additional File 2: Fig. S15A, $r = 0.96$, $p < 2.2e\text{-}16$), confirming METER-quant's capability to provide precise TC quantification. When considering patients' serial time points, METER-quant showed expected TC dynamics, confirming its reliability for longitudinal disease monitoring (Additional File 2: Fig. S15B). Specifically, METER-quant revealed a significant decrease in ctDNA levels from BL to C2D1 (paired $p = 0.005$), and an overall rebound at disease progression when compared to C2D1 (paired $p < 0.001$) or the most recent prior time point for each patient (paired $p < 0.001$). Coherent results were provided by METER-detect at serial time points (Additional File 2: Fig. S15C). As for the MIMESIS-1, we applied METER-subtype to samples from HER2- BC patients, using available IHC on the most recent archived sample as BC subtype ground truth. Considering 48 samples with METER-quant ≥ 5%, METER-subtype showed an accuracy of 0.90 (95% CI: 0.77–0.97) with a CR of 0.85, consistent with the MIMESIS-1 analysis (Additional File 2: Fig. S15D). Statistical significance was however not reached, likely due to the limited number of ER- samples ($p = 0.15$). Indeed, when combining samples with METER-quant TC ≥ 5% from the two datasets, for a total of 80 ER+/HER2- and 12 ER-/HER2- samples, METER-subtype demonstrated significant classification accuracy of 0.93 (95% CI: 0.85–0.97, $p = 0.03$) misclassifying 6 out of 92 samples (Additional File 2: Fig. S15E, G and Additional File 1: Table S8, S11). In Fig. 6A, ctDNA detection for each patient over multiple time points is shown with relevant clinical events from study entry to progression, death, or last follow-up. Key clinicopathological characteristics of patients are annotated for a comprehensive dataset overview. Notably, most patients with METER- samples at both BL and C2D1 (8 out of 14) did not experience disease progression from study entry. Among the remaining 6 progressors, three showed disease progression after the median follow-up of those who remained progression-free (median follow-up time = 24 months). In contrast, 14 out of 16 patients with METER+ samples at BL and C2D1 progressed, with 9 within 6 months. Importantly, among 19 patients who progressed and had data for at least 1 monitoring time point (I1–I3), 11 resulted METER+ at least once before progression, suggesting METER-detect's utility in providing anticipated detection of progression. Since the MIMESIS-2 study was primarily designed to monitor patients on first- or second-line treatment with HR+/HER2- mBC, we specifically focused on examining the association between METER-detect and PFS within the homogeneous subset of HR+/HER2- patients included in the cohort. (Fig. 6B–E and Additional File 2: Fig. S16-18; results for the full cohort are reported in Additional File 2: Fig. S19-21). METER-detect confirmed enhanced detection sensitivity and more effective prognostic stratification in terms of both PFS and OS compared to ichorCNA, even when limiting the analysis to ichorCNA- patients (Fig. 6B–E and Additional File 2: Fig. S16–18), and associations remained significant after adjusting for clinically relevant covariates (Additional File 1: Table S12). Notably, although significant stratification was not observed considering ctDNA status at the second radiological evaluation (I2, Additional File 2: Fig. S17A–B), METER-detect demonstrated a significant association with PFS and OS considering samples at the third radiological evaluation (I3, Fig. 6E and Additional File 2: Fig. S17C–D), highlighting METER-detect as a tool for providing evidence of disease progression earlier than imaging. ctDNA detection concordance by ichorCNA and METER-detect for ER+/HER2- patients in the MIMESIS-2 is reported in Additional File 2: Fig. S22.

Discussion

In the context of precision oncology, improving ctDNA analysis through robust, reproducible and scalable methods offers significant clinical value. To address this critical clinical need, we here introduce and qualify METER for the comprehensive ctDNA analysis from low-pass whole methylome sequencing of plasma samples. METER leverages genomically pervasive and tumor-type prevalent [27, 50, 51] methylation signals for accurate quantification and sensitive detection of ctDNA in challenging low TC ranges, as well as for ctDNA-based tumor subtyping, through a simple, robust, and cost-effective strategy. This enables non-invasive disease and tumor phenotype monitoring and prognostic stratification, with strong potential for integration into clinical routine, where such applications remain limited. Our approach is cost-effective as it does not involve the enrichment of specific regions before sequencing, requiring a small amount (10–20ng) of input DNA. In contrast to most DNA methylation-based methods relying on depth of coverage of specific sites and/or regions (vertical-wise analysis), our approach is flexible and open to the integration of multimodal analyses, such as CNA profiling (or other genome-wide patterns). It is patients' tumor tissue-agnostic (e.g., not depending on the analysis of matched tumor tissue-specific alterations), and exclusively based on pre-defined DNA methylation markers (DMR and DMS).

There are relevant considerations to be mentioned regarding the methylation markers used by METER and their potential limitation. First, the markers are defined based on group-level differential analysis, which cannot fully capture the potential intratumoral DNA methylation heterogeneity. Although this may impact METER's performance, our algorithm for selecting informative DMR and DMS is designed to identify clonal, tumor-specific methylation changes, providing robust markers

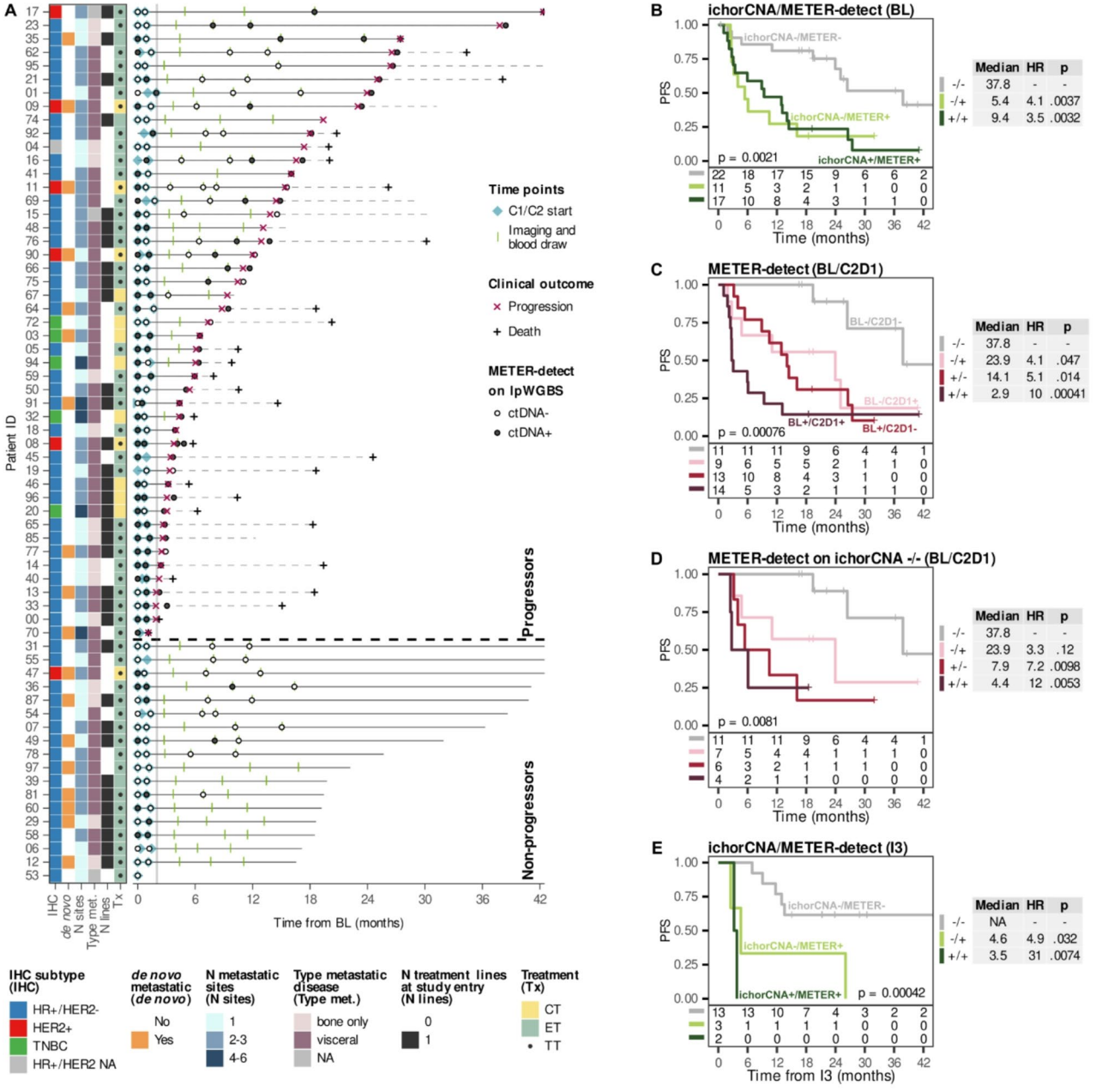

Fig. 6 Validation of METER predictions on the MIMESIS-2 dataset. **A** Swimmer plot showing clinical trajectories and ctDNA detection in plasma samples by METER-detect for patients from the MIMESIS-2 cohort, alongside key clinicopathological characteristics and clinical outcome. **B** Kaplan-Meier curves showing PFS of HR+/HER2- patients from the MIMESIS-2 cohort, stratified by combined ichorCNA [16] and METER-detect ctDNA detection at BL (-/-, -/+, +/+). p values shown in Kaplan-Meier curves are from the Log-Rank test. **C** and **D** Kaplan-Meier curves showing PFS of HR+/HER2- patients from the MIMESIS-2 cohort, stratified according to ctDNA detection by METER-detect at BL and C2D1 time points (-/-, -/+, +/- or +/+); **C** includes all HR+/HER2- patients with matched BL and C2D1 time points, while (**D**) includes only ichorCNA -/- patients at BL/C2D1 time points. **E** Kaplan-Meier curves showing PFS from I3 time point of HR+/HER2- patients from the MIMESIS-2 cohort, stratified by combined ichorCNA and METER-detect ctDNA detection at I3 (-/-, -/+, +/+). p values shown in Kaplan-Meier curves are from the Log-Rank test

that are reasonably minimally affected by such heterogeneity. Second, the markers are defined based on primary tumor tissues. Although marker selection criteria suggest that these alterations should reflect events arising early in tumorigenesis, we cannot exclude the possibility that treatment-induced transdifferentiation may substantially disrupt lineage-specific DNA methylation patterns [11], thereby potentially affecting the performance of METER's predictions.

Importantly, METER is a simple and direct method for measuring TC and detecting ctDNA, based on the measurement of the proportion of tumor-like CpG sites

(pTS) and tumor-like sequence reads (pTR), reflecting intra-read versus intra-region signal coherence. While machine learning approaches or optimization algorithms can be effective for TC assessment [16–18, 23], they may suffer from poor reproducibility and dependency on input parameters. On the contrary, METER minimalist strategy requires lpWGBS data training limited to control samples (i.e., pTR mean and variance that are provided in METER-detect as precomputed values), thus making it amenable to the use in clinical practice.

We evaluated the technical performance and clinical significance of our approach by applying METER to 338 plasma samples from 124 patients with mBC, primarily on first- or second-line treatment, enrolled in two independent studies. The MIMESIS-1 study was used to test and qualify our strategy, while the MIMESIS-2 served as a validation cohort and to assess our method for disease monitoring, including a median of 3 time points per patient. We observed excellent consistency in TC level quantification by METER-quant and the state-of-the-art tool ichorCNA [16] on tumor samples in both datasets. Importantly, when applied to ichorCNA-undetected samples (TC by ichorCNA < 3%) from both the MIMESIS-1 and MIMESIS-2, METER-detect identified tumor signal in around half of these cases and demonstrated superior sensitivity compared to CancerDetector [42]. Based on an extensive in silico study and a LOOCV approach on control samples, METER achieves a lower detection limit of approximately 1% while maintaining an FDR < 5%. Exploiting selected DMR as a proxy of specific tumor transcriptional programs, we explored the applicability of METER-subtype to accurately infer tumor ER status from ctDNA in HER2- patients. Combining samples with METER-quant ≥ 5% from both the MIMESIS-1 and MIMESIS-2 cohorts and considering IHC on the most recent archived sample as ground truth, METER-subtype achieved a significant classification accuracy of 0.93 (95% CI (0.85–0.97)) and provided consistent prediction for all evaluable BL-Prog samples derived from the same patient (Additional File 2: Fig. S14E and S15F). Of note, METER-subtype demonstrated superior and comparable performance compared to Griffin [23] and cfDeconvolve [42], respectively. For Griffin, the original publication reported an accuracy of 0.92 (95% CI (0.82–1)) for predicting ER status. However, it's important to note that Griffin was not originally evaluated in bisulfite-treated samples, and that the current study includes samples with significantly lower TC compared to the original Griffin study (Additional File 2: Fig. S23), which may explain the lower performance observed. The possibility of inferring clinically relevant transcriptional programs from DNA features estimated from low-pass WGS was recently shown, including ER status and RB-loss [52]. However, the authors reported a failure rate of up to 20% for the method in the case of TC in the range of 5–10% and lower accuracy (AUC = 0.8) compared to this and the previous study [23] for inferring ER status. Since METER-subtype accuracy depends on TC (Additional File 2: Fig. S14B, C, F, and S15G), it holds significant promise for advanced treatment settings, where more frequent ER loss is expected due to resistance mechanisms from prolonged exposure to endocrine therapy and/or chemotherapy [53–57], and especially in case of challenging-to-access metastatic sites such as brain metastases [58].

In this study, we extensively demonstrated the clinical relevance of our method using curated clinical data from the MIMESIS-1 and MIMESIS-2. Considering patients' serial time points, METER-quant demonstrated expected TC modulation reflecting treatment responses and disease progression patterns, underscoring its applicability in tracking ctDNA dynamics over time.

Overall, METER-detect demonstrated enhanced sensitivity in ctDNA detection and more effective prognostic stratification for PFS and OS compared to ichorCNA, especially when considering BL and early dynamic changes in ctDNA (BL/C2D1) for stratification. This association persisted even when the analysis was restricted to ichorCNA- patients with TC below 3% and across both the clinically heterogeneous cohort MIMESIS-1 and the more homogeneous subset of first- or second-line HR+/HER2- patients from the MIMESIS-2.

Moreover, the specific design of the MIMESIS-2, including multiple longitudinal samples corresponding to radiological evaluations (I1–I3), allowed us to demonstrate METER-detect as a valuable tool for ctDNA surveillance during treatment to anticipate disease progression.

We further validated METER-detect applicability in low TC settings by demonstrating its association with matched CTC [29–31], specifically in samples with TC < 3%, undetected by ichorCNA. Notably, ctDNA presence assessed by METER-detect exhibited superior prognostic stratification compared to CTCs, extensively demonstrated as a clinically validated non-invasive prognostic biomarker in BC [59–61]. It is important to note that, while ichorCNA is completely tumor-type agnostic, METER relies on robust predefined tumor-type-specific DMS and DMR, which are critical for its performance. Consequently, the extension of METER applicability to other tumor types depends on the identification of reliable, case-specific methylation markers, which may not always be readily available. The applicability of METER to BL and on treatment plasma cfDNA profiled with low-pass methylome sequencing was evidenced by the recent investigation on patients with metastatic colorectal cancer enrolled in the VALENTINO phase II trial [62] that showed consistent results in terms of ctDNA detection,

tumor content monitoring and patients' prognostic stratification, supporting the generalizability of the approach for the analysis of other tumor types [63]. In addition, we demonstrated the feasibility of using METER with DMS and DMR identified from array data [51], enabling broader data accessibility for other tumor types compared to WGBS. Overall, we observed consistent results with those obtained from WGBS-based DMS and DMR, though with reduced performance in patient stratification, likely due to the lower quantity and reliability of array-based DMR (Additional File 2: Supplementary Text and Fig. S24–26). Another aspect to consider is that the use of lpWGBS with METER is limited in early disease settings, spanning extremely low TC levels, for applications like minimal residual disease (MRD) or monitoring during adjuvant treatment. Common strategies in these contexts include tumor-informed analyses, high-coverage sequencing of large DNA/DNA-methylation regions, or WGS [64–66]. As proof of concept in early-stage disease, we analyzed pre-surgical plasma samples from four early CRC patients. The analysis revealed significantly higher levels of pTR (the metric used by METER-detect) compared to controls, supporting METER's suitability for early-stage cancer detection and further demonstrating its applicability beyond BC.

In addition, while intrinsically limited by in silico modeling, our synthetic study indicates that METER-detect can achieve detection of ~1% TC at ~0.7x coverage, and ~0.1% TC at ~4x. These findings highlight that METER's performance can be substantially improved with a moderate increase in sequencing cost, while remaining tumor-tissue agnostic and independent from machine learning classifiers. More specifically, considering that library preparation cost is invariable and that the sequencing expenses scale approximately linearly with coverage, we estimate that achieving this order-of-magnitude improvement in detectable TC would require approximately a doubling of the total costs.

Conclusions

METER is a novel, robust, and cost-effective tool enhancing ctDNA analysis in challenging scenarios like metastatic disease monitoring during first- or second-line therapy, where TC levels are typically low. Based on strong and independent associations with clinically relevant factors across two independent clinical studies, METER-detect may serve as a tumor tissue-agnostic and practical method for classifying plasma samples by ctDNA presence. Additionally, METER provides accurate tumor subtyping, enabling comprehensive ctDNA analysis. Importantly, our approach is generalizable to other tumor types or subtypes using tumor-specific DMS and DMR, expanding its clinical applications.

Abbreviations

AUC	Area under the curve
BC	Breast cancer
BL	Baseline
cfDNA	Cell-free DNA
CNA	Copy number alteration
CR	Call rate
CTC	Circulating tumor cells
DMR	Differentially methylated region
DMS	Differentially methylated site
ER	Estrogen receptor
FDR	False discovery rate
HER2	Human epidermal growth factor receptor 2
HR	Hazard ratio
HR+	Hormone receptor positive
IHC	Immunohistochemistry
lpWGBS	Low-pass whole genome bisulfite sequencing
lpWGS	Low-pass whole genome sequencing
MAE	Median absolute error
mBC	Metastatic breast cancer
MRD	Minimal residual disease
OS	Overall survival
PCR	Polymerase chain reaction
PFS	Progression-free survival
pTR	Proportion of tumor-like reads
pTS	Proportion of tumor-like CpG sites
ROC	Receiver operating characteristic
RPC	Robust partial correlation
s-ctDNA	Surrogate circulating tumor DNA
TC	Tumor content
TNBC	Triple negative breast cancer
WGBS	Whole genome bisulfite sequencing
WGS	Whole genome sequencing

Supplementary Information

The online version contains supplementary material available at https://doi.org/10.1186/s13073-026-01603-3.

Supplementary Material 1. Additional File 1: Supplementary Tables.

Supplementary Material 2. Additional File 2: Supplementary Text and Supplementary Figures.

Acknowledgements

The authors thank the members of the bioinformatics unit and the translational research unit of the Hospital of Prato (Prato) and the laboratory of computational and functional oncology (University of Trento) for fruitful discussions. The authors thank Roberto Bertorelli and Veronica De Sanctis from the NGS core facility of CIBIO (University of Trento) for their help on setting up the sequencing experiments. The authors thank all the patients who participated in the studies and their families.

Authors' contributions

Conceptualization: MB, FD, MPMethodology: MB, FD, MP, FG, ANSoftware: MPFormal analysis: MP, CBInvestigation: MP, FG, AN, CBResources: MB, FD, SDD, LL, MP, GS, ER, LM, LBData Curation: FG, AN, CB, MP, DRWriting - Original Draft: MB, FD, MPWriting - Review & Editing: MP, FG, AN, CB, DR, SDD, GMF, LL, MP, GS, ER, IM, EM, LM, LB, FD, MBVisualization: MP, MBSupervision: MB, FD, LB, LMProject administration: MB, FD, LM, LBFunding acquisition: MB, FD, LBAll authors read and approved the final manuscript.

Funding

The research leading to these results has received funding from AIRC under IG 2022 - ID. 27036 P.I. Benelli Matteo; the Italian Minister of Health under Ricerca Finalizzata 2018 - GR-2018-12365195 - P.I. Benelli Matteo; AIRC under IG 2023 - ID. 29370 - P.I. Francesca Demichelis; and Fondazione "Sandro Pitigliani" per la lotta contro i tumori ONLUS.

Data availability

The datasets generated and analysed during the current study, i.e. Bismark [36] methylation calls on cfDNA lpWGBS samples from the MIMESIS-1 and MIMESIS-2 cohorts and BAM files of control samples are available on Zenodo [67]. Sequence files from MIMESIS-1 and MIMESIS-2 (patients) are not publicly available, as data sharing was not explicitly included in the informed consent. METER was developed as a package for R and is available under the MIT license [68].

Declarations

Ethics approval and consent to participate

The trials included in this study received approval from the local institutional ethics committee of the Hospital of Prato and by the Area Vasta Toscana Centro and local Ethics Committee (CEAVC 15108; CEAVC 11252), in accordance with Helsinki Declaration. Written informed consent was prospectively obtained from all patients participating in these trials.

Consent for publication

Not applicable.

Competing interests

Authors declare that they have no competing interests related to this work. Out of this work, ER reports honoraria from Eisai; travel grants from Pfizer, Gilead Sciences; LM reports Honoraria from Pfizer, Novartis, Seagen; consulting or advisory role from Pfizer, Novartis, Seagen, Roche, Menarini Group; research funding from Pfizer, Novartis; travel, accommodations, expenses from Roche, Janssen, Gilead Sciences, Menarini Group; LB reports personal financial interests (Honoraria, consultancy or advisory role) from Amgen, AstraZeneca, Boehringer-Ingelheim, Daiichi-Sankyo, Eisai, Exact Sciences, Gilead, Lilly, Menarini, Novartis, Pfizer, Pierre Fabre, Roche, Sanofi, SeaGen; institutional financial interests from Celgene, Genomic Health, Novartis; travel grant from AstraZeneca, Daiichi-Sankyo. The remaining authors declare that they have no competing interests.

Received: 1 August 2025 / Accepted: 27 January 2026
Published online: 03 February 2026

References

1. Cescon DW, Bratman SV, Chan SM, Siu LL. Circulating tumor DNA and liquid biopsy in oncology. Nat Cancer. 2020;1:276–90. https://doi.org/10.1038/s43018-020-0043-5.
2. Siravegna G, Marsoni S, Siena S, Bardelli A. Integrating liquid biopsies into the management of cancer. Nat Rev Clin Oncol. 2017;14:531–48. https://doi.org/10.1038/nrclinonc.2017.14.
3. Gouda MA, Janku F, Wahida A, Buschhorn L, Schneeweiss A, Abdel Karim N, et al. Liquid biopsy response evaluation criteria in solid tumors (LB-RECIST). Ann Oncol. 2024;35:267–75. https://doi.org/10.1016/j.annonc.2023.12.007.
4. Ignatiadis M, Sledge GW, Jeffrey SS. Liquid biopsy enters the clinic - implementation issues and future challenges. Nat Rev Clin Oncol. 2021;18:297–312. https://doi.org/10.1038/s41571-020-00457-x.
5. Reichert ZR, Morgan TM, Li G, Castellanos E, Snow T, Dall'Olio FG, et al. Prognostic value of plasma Circulating tumor DNA fraction across four common cancer types: a real-world outcomes study. Ann Oncol [Internet]. 2022. https://doi.org/10.1016/j.annonc.2022.09.163.
6. Stover DG, Parsons HA, Ha G, Freeman SS, Barry WT, Guo H, et al. Association of cell-free DNA tumor fraction and somatic copy number alterations with survival in metastatic triple-negative breast cancer. J Clin Oncol. 2018;36:543–53. https://doi.org/10.1200/JCO.2017.76.0033.
7. Dawson S-J, Tsui DWY, Murtaza M, Biggs H, Rueda OM, Chin S-F, et al. Analysis of circulating tumor DNA to monitor metastatic breast cancer. N Engl J Med. 2013;368:1199–209. https://doi.org/10.1056/NEJMoa1213261.
8. Tsui DWY, Cheng ML, Shady M, Yang JL, Stephens D, Won H, et al. Tumor fraction-guided cell-free DNA profiling in metastatic solid tumor patients. Genome Med. 2021;13:96. https://doi.org/10.1186/s13073-021-00898-8.
9. Husain H, Pavlick DC, Fendler BJ, Madison RW, Decker B, Gjoerup O, et al. Tumor fraction correlates with detection of actionable variants across >23,000 Circulating tumor DNA samples. JCO Precis Oncol. 2022;6:e2200261. https://doi.org/10.1200/PO.22.00261.
10. Beltran H, Romanel A, Conteduca V, Casiraghi N, Sigouros M, Franceschini GM, et al. Circulating tumor DNA profile recognizes transformation to castration-resistant neuroendocrine prostate cancer. J Clin Invest. 2020;130:1653–68. https://doi.org/10.1172/JCI131041.
11. Franceschini GM, Quaini O, Mizuno K, Orlando F, Ciani Y, Ku S-Y, et al. Noninvasive detection of neuroendocrine prostate cancer through targeted Cell-free DNA methylation. Cancer Discov. 2024;14:424–45. https://doi.org/10.1158/2159-8290.CD-23-0754.
12. Romanel A, Gasi Tandefelt D, Conteduca V, Jayaram A, Casiraghi N, Wetterskog D, et al. Plasma AR and abiraterone-resistant prostate cancer. Sci Transl Med. 2015;7:312re10-312re10. https://doi.org/10.1126/scitranslmed.aac9511.
13. Orlando F, Romanel A, Trujillo B, Sigouros M, Wetterskog D, Quaini O, et al. Allele-informed copy number evaluation of plasma DNA samples from metastatic prostate cancer patients: the PCF_SELECT consortium assay. NAR Cancer. 2022;4:zcac016. https://doi.org/10.1093/narcan/zcac016.
14. Rolfo CD, Madison RW, Pasquina LW, Brown DW, Huang Y, Hughes JD, et al. Measurement of ctDNA tumor fraction identifies informative negative liquid biopsy results and informs value of tissue confirmation. Clin Cancer Res. 2024;30:2452–60. https://doi.org/10.1158/1078-0432.CCR-23-3321.
15. Rose Brannon A, Jayakumaran G, Diosdado M, Patel J, Razumova A, Hu Y, et al. Enhanced specificity of clinical high-sensitivity tumor mutation profiling in cell-free DNA via paired normal sequencing using MSK-ACCESS. Nat Commun. 2021;12:3770. https://doi.org/10.1038/s41467-021-24109-5.
16. Adalsteinsson VA, Ha G, Freeman SS, Choudhury AD, Stover DG, Parsons HA, et al. Scalable whole-exome sequencing of cell-free DNA reveals high concordance with metastatic tumors. Nat Commun. 2017;8:1324. https://doi.org/10.1038/s41467-017-00965-y.
17. Cristiano S, Leal A, Phallen J, Fiksel J, Adleff V, Bruhm DC, et al. Genome-wide cell-free DNA fragmentation in patients with cancer. Nature. 2019;570:385–9. https://doi.org/10.1038/s41586-019-1272-6.
18. Shen SY, Singhania R, Fehringer G, Chakravarthy A, Roehrl MHA, Chadwick D, et al. Sensitive tumour detection and classification using plasma cell-free DNA methylomes. Nature. 2018;563:579–83. https://doi.org/10.1038/s41586-018-0703-0.
19. Bianchini G, Malorni L, Arpino G, Zambelli A, Puglisi F, Mastro LD, et al. Abstract GS3-07: Circulating tumor DNA (ctDNA) dynamics in patients with hormone receptor positive (HR+)/HER2 negative (HER2-) advanced breast cancer (aBC) treated in first line with ribociclib (R) and letrozole (L) in the BioItaLEE trial. Cancer Res. 2022;82:GS3-07-GS3-07. https://doi.org/10.1158/1538-7445.SABCS21-GS3-07.
20. Wu A, Cremaschi P, Wetterskog D, Conteduca V, Franceschini GM, Kleftogiannis D, et al. Genome-wide plasma DNA methylation features of metastatic prostate cancer. J Clin Invest. 2020;130:1991–2000. https://doi.org/10.1172/JCI130887.
21. Baca SC, Seo J-H, Davidsohn MP, Fortunato B, Semaan K, Sotudian S, et al. Liquid biopsy epigenomic profiling for cancer subtyping. Nat Med. 2023;29:2737–41. https://doi.org/10.1038/s41591-023-02605-z.
22. Bie F, Wang Z, Li Y, Guo W, Hong Y, Han T, et al. Multimodal analysis of cell-free DNA whole-methylome sequencing for cancer detection and localization. Nat Commun. 2023;14:6042. https://doi.org/10.1038/s41467-023-41774-w.
23. Doebley A-L, Ko M, Liao H, Cruikshank AE, Santos K, Kikawa C, et al. A framework for clinical cancer subtyping from nucleosome profiling of cell-free DNA. Nat Commun. 2022;13:7475. https://doi.org/10.1038/s41467-022-35076-w.
24. Stanley KE, Jatsenko T, Tuveri S, Sudhakaran D, Lannoo L, Van Calsteren K, et al. Cell type signatures in cell-free DNA fragmentation profiles reveal disease biology. Nat Commun. 2024;15:2220. https://doi.org/10.1038/s41467-024-46435-0.
25. Chan KCA, Jiang P, Chan CWM, Sun K, Wong J, Hui EP, et al. Noninvasive detection of cancer-associated genome-wide hypomethylation and copy number aberrations by plasma DNA bisulfite sequencing. Proc Natl Acad Sci U S A. 2013;110:18761–8. https://doi.org/10.1073/pnas.1313995110.
26. Sun K, Jiang P, Chan KCA, Wong J, Cheng YKY, Liang RHS, et al. Plasma DNA tissue mapping by genome-wide methylation sequencing for noninvasive prenatal, cancer, and transplantation assessments. Proc Natl Acad Sci U S A. 2015;112:E5503-5512. https://doi.org/10.1073/pnas.1508736112.
27. Romagnoli D, Nardone A, Galardi F, Paoli M, De Luca F, Biagioni C, et al. MIMESIS: minimal DNA-methylation signatures to quantify and classify tumor signals in tissue and cell-free DNA samples. Brief Bioinform. 2023. https://doi.org/10.1093/bib/bbad015.
28. Scandino R, Nardone A, Casiraghi N, Galardi F, Genovese M, Romagnoli D, et al. Enabling sensitive and precise detection of ctDNA through somatic copy

number aberrations in breast cancer. Npj Breast Cancer. 2025;11:25. https://doi.org/10.1038/s41523-025-00739-6.
29. De Luca F, Rotunno G, Salvianti F, Galardi F, Pestrin M, Gabellini S, et al. Mutational analysis of single circulating tumor cells by next generation sequencing in metastatic breast cancer. Oncotarget. 2016;7:26107–19. https://doi.org/10.18632/oncotarget.8431.
30. Galardi F, De Luca F, Biagioni C, Migliaccio I, Curigliano G, Minisini AM, et al. Circulating tumor cells and palbociclib treatment in patients with ER-positive, HER2-negative advanced breast cancer: results from a translational sub-study of the TREnd trial. Breast Cancer Res. 2021;23:38. https://doi.org/10.1186/s13058-021-01415-w.
31. Pestrin M, Salvianti F, Galardi F, De Luca F, Turner N, Malorni L, et al. Heterogeneity of PIK3CA mutational status at the single cell level in circulating tumor cells from metastatic breast cancer patients. Mol Oncol. 2015;9:749–57. https://doi.org/10.1016/j.molonc.2014.12.001.
32. Di Donato S, Malinconi S, Galardi F, Cantafio S, Orioli T, Biagioni C, et al. 774p clinical and molecular profiling of high-risk localized colorectal cancer (CRC) in the LIBIMET trial. Ann Oncol. 2025;36:S500. https://doi.org/10.1016/j.annonc.2025.08.1347.
33. Achinger-Kawecka J, Valdes-Mora F, Luu P-L, Giles KA, Caldon CE, Qu W, et al. Epigenetic reprogramming at estrogen-receptor binding sites alters 3D chromatin landscape in endocrine-resistant breast cancer. Nat Commun. 2020;11:320. https://doi.org/10.1038/s41467-019-14098-x.
34. Danecek P, Bonfield JK, Liddle J, Marshall J, Ohan V, Pollard MO, et al. Twelve years of SAMtools and BCFtools. Gigascience. 2021;10:giab008. https://doi.org/10.1093/gigascience/giab008.
35. Ewels PA, Peltzer A, Fillinger S, Patel H, Alneberg J, Wilm A, et al. The nf-core framework for community-curated bioinformatics pipelines. Nat Biotechnol. 2020;38:276–8. https://doi.org/10.1038/s41587-020-0439-x.
36. Krueger F, Andrews SR. Bismark: a flexible aligner and methylation caller for Bisulfite-Seq applications. Bioinformatics. 2011;27:1571–2. https://doi.org/10.1093/bioinformatics/btr167.
37. Krueger F. Trim Galore. https://www.bioinformatics.babraham.ac.uk/projects/trim_galore.
38. Benelli M, Franceschini GM, Magi A, Romagnoli D, Biagioni C, Migliaccio I, et al. Charting differentially methylated regions in cancer with Rocker-meth. Commun Biol. 2021;4:1249. https://doi.org/10.1038/s42003-021-02761-3.
39. Brinkman AB, Nik-Zainal S, Simmer F, Rodríguez-González FG, Smid M, Alexandrov LB, et al. Partially methylated domains are hypervariable in breast cancer and fuel widespread CpG island hypermethylation. Nat Commun. 2019;10:1749. https://doi.org/10.1038/s41467-019-09828-0.
40. Loyfer N, Magenheim J, Peretz A, Cann G, Bredno J, Klochendler A, et al. A DNA methylation atlas of normal human cell types. Nature. 2023;613:355–64. https://doi.org/10.1038/s41586-022-05580-6.
41. Singer BD. A practical guide to the measurement and analysis of DNA methylation. Am J Respir Cell Mol Biol. 2019;61:417–28. https://doi.org/10.1165/rcmb.2019-0150TR.
42. Li W, Li Q, Kang S, Same M, Zhou Y, Sun C, et al. CancerDetector: ultrasensitive and non-invasive cancer detection at the resolution of individual reads using cell-free DNA methylation sequencing data. Nucleic Acids Res. 2018;46:e89. https://doi.org/10.1093/nar/gky423.
43. Teschendorff AE, Breeze CE, Zheng SC, Beck S. A comparison of reference-based algorithms for correcting cell-type heterogeneity in epigenome-wide association studies. BMC Bioinformatics. 2017;18:105. https://doi.org/10.1186/s12859-017-1511-5.
44. Chemi F, Pearce SP, Clipson A, Hill SM, Conway A-M, Richardson SA, et al. cfDNA methylome profiling for detection and subtyping of small cell lung cancers. Nat Cancer. 2022;3:1260–70. https://doi.org/10.1038/s43018-022-00415-9.
45. Wei Q, Jin C, Wang Y, Guo S, Guo X, Liu X, et al. A computational framework to unify orthogonal information in DNA methylation and copy number aberrations in cell-free DNA for early cancer detection. Brief Bioinform. 2022;23:bbac200. https://doi.org/10.1093/bib/bbac200.
46. Thomas-Bonafos T, Pierga JY, Bidard F-C, Cabel L, Kiavue N. Circulating tumor cells in breast cancer: clinical validity and utility. NPJ Breast Cancer. 2024;10:103. https://doi.org/10.1038/s41523-024-00706-7.
47. Cristofanilli M, Budd GT, Ellis MJ, Stopeck A, Matera J, Miller MC, et al. Circulating tumor cells, disease progression, and survival in metastatic breast cancer. N Engl J Med. 2004;351:781–91. https://doi.org/10.1056/NEJMoa040766.
48. Lindström LS, Karlsson E, Wilking UM, Johansson U, Hartman J, Lidbrink EK, et al. Clinically used breast cancer markers such as estrogen receptor, progesterone receptor, and human epidermal growth factor receptor 2 are unstable throughout tumor progression. J Clin Oncol. 2012;30:2601–8. https://doi.org/10.1200/JCO.2011.37.2482.
49. Morganti S, Parsons HA, Lin NU, Grinshpun A. Liquid biopsy for brain metastases and leptomeningeal disease in patients with breast cancer. NPJ Breast Cancer. 2023;9:43. https://doi.org/10.1038/s41523-023-00550-1.
50. Benelli M, Romagnoli D, Demichelis F. Tumor purity quantification by clonal DNA methylation signatures. Bioinformatics. 2018. https://doi.org/10.1093/bioinformatics/bty011.
51. Hoadley KA, Yau C, Hinoue T, Wolf DM, Lazar AJ, Drill E, et al. Cell-of-origin patterns dominate the molecular classification of 10,000 tumors from 33 types of cancer. Cell. 2018;173:291-304.e6. https://doi.org/10.1016/j.cell.2018.03.022.
52. Prat A, Brasó-Maristany F, Martínez-Sáez O, Sanfeliu E, Xia Y, Bellet M, et al. Circulating tumor DNA reveals complex biological features with clinical relevance in metastatic breast cancer. Nat Commun. 2023;14:1157. https://doi.org/10.1038/s41467-023-36801-9.
53. Schrijver WAME, Suijkerbuijk KPM, van Gils CH, van der Wall E, Moelans CB, van Diest PJ. Receptor conversion in distant breast cancer metastases: a systematic review and meta-analysis. J Natl Cancer Inst. 2018;110:568–80. https://doi.org/10.1093/jnci/djx273.
54. Shiino S, Ball G, Syed BM, Kurozumi S, Green AR, Tsuda H, et al. Prognostic significance of receptor expression discordance between primary and recurrent breast cancers: a meta-analysis. Breast Cancer Res Treat. 2022;191:1–14. https://doi.org/10.1007/s10549-021-06390-6.
55. Aftimos P, Oliveira M, Irrthum A, Fumagalli D, Sotiriou C, Gal-Yam EN, et al. Genomic and transcriptomic analyses of breast cancer primaries and matched metastases in AURORA, the Breast International Group (BIG) molecular screening initiative. Cancer Discov. 2021;11:2796–811. https://doi.org/10.1158/2159-8290.CD-20-1647.
56. Garcia-Recio S, Hinoue T, Wheeler GL, Kelly BJ, Garrido-Castro AC, Pascual T, et al. Multiomics in primary and metastatic breast tumors from the AURORA US network finds microenvironment and epigenetic drivers of metastasis. Nat Cancer. 2023;4:128–47. https://doi.org/10.1038/s43018-022-00491-x.
57. Cejalvo JM, de Dueñas EM, Galván P, García-Recio S, Gasión OB, Paré L, et al. Intrinsic subtypes and gene expression profiles in primary and metastatic breast cancer. Cancer Res. 2017;77:2213–21. https://doi.org/10.1158/0008-5472.CAN-16-2717.
58. Hulsbergen AFC, Claes A, Kavouridis VK, Ansaripour A, Nogarede C, Hughes ME, et al. Subtype switching in breast cancer brain metastases: a multicenter analysis. Neuro-Oncology. 2020;22:1173–81. https://doi.org/10.1093/neuonc/noaa013.
59. Bidard F-C, Peeters DJ, Fehm T, Nolé F, Gisbert-Criado R, Mavroudis D, et al. Clinical validity of circulating tumour cells in patients with metastatic breast cancer: a pooled analysis of individual patient data. Lancet Oncol. 2014;15(4):406. https://doi.org/10.1016/S1470-2045(14)70069-5.
60. Cabel L, Proudhon C, Gortais H, Loirat D, Coussy F, Pierga J-Y, et al. Circulating tumor cells: clinical validity and utility. Int J Clin Oncol. 2017;22(3):421. https://doi.org/10.1007/s10147-017-1105-2.
61. Sparano J, O'Neill A, Alpaugh K, Wolff AC, Northfelt DW, Dang CT, et al. Association of circulating tumor cells with late recurrence of estrogen receptor-positive breast cancer: a secondary analysis of a randomized clinical trial. JAMA Oncol. 2018;4:1700. https://doi.org/10.1001/jamaoncol.2018.2574.
62. Pietrantonio F, Morano F, Corallo S, Miceli R, Lonardi S, Raimondi A, et al. Maintenance therapy with panitumumab alone vs panitumumab plus fluorouracil-leucovorin in patients with RAS wild-type metastatic colorectal cancer: a phase 2 randomized clinical trial. JAMA Oncol. 2019;5:1268. https://doi.org/10.1001/jamaoncol.2019.1467.
63. Manca P, Paoli M, Galardi F, Morano F, Di Donato S, Biganzoli L, et al. CtDNA detection with low-pass whole genome bisulfite sequencing in RAS wild-type metastatic colorectal cancer: an exploratory objective of the VALENTINO trial. Clin Cancer Res Off J Am Assoc Cancer Res. 2025. https://doi.org/10.1158/1078-0432.CCR-25-2773.
64. Zviran A, Schulman RC, Shah M, Hill STK, Deochand S, Khamnei CC, et al. Genome-wide cell-free DNA mutational integration enables ultra-sensitive cancer monitoring. Nat Med. 2020;26:1114. https://doi.org/10.1038/s41591-020-0915-3.
65. Jamshidi A, Liu MC, Klein EA, Venn O, Hubbell E, Beausang JF, et al. Evaluation of cell-free DNA approaches for multi-cancer early detection. Cancer Cell. 2022;40:1537-1549.e12. https://doi.org/10.1016/j.ccell.2022.10.022.
66. Liu MCC, Oxnard GRR, Klein EAA, Swanton C, Seiden MVV, Cummings SR, et al. Sensitive and specific multi-cancer detection and localization using

methylation signatures in cell-free DNA. Ann Oncol. 2020;31:745. https://doi.org/10.1016/j.annonc.2020.02.011.
67. Paoli M. The MIMESIS dataset. https://doi.org/10.5281/zenodo.17781295.
68. Paoli M. The METER computational framework. https://github.com/caos-lab-unifi/METER.

Publisher's Note